AECL EACL

CA9700642

AECL-11592, COG-96-273

Modelling the Effects of Porous and Semi-Permeable Layers on Corrosion Processes

Modélisation des effets des couches poreuses et semi-perméables sur les processus de corrosion

F. King, M. Kolář, D.W. Shoesmith

September 1996 septembre

MODELLING THE EFFECTS OF POROUS AND SEMI-PERMEABLE LAYERS ON CORROSION PROCESSES

by

F. King, M. Kolář and D. W. Shoesmith

This report was presented as paper no. 380 at CORROSION/96, Denver, CO, 25-29 March, 1996.

Whiteshell Laboratories
Pinawa, Manitoba, Canada R0E 1L0
1996

AECL-11592
COG-96-273

MODELLING THE EFFECTS OF POROUS AND SEMI-PERMEABLE LAYERS ON CORROSION PROCESSES

by

F. King, M. Kolář and D.W. Shoesmith

ABSTRACT

Porous and semi-permeable layers play a role in many corrosion processes. Porous layers may simply affect the rate of corrosion by affecting the rate of mass transport of reactants and products to and from the corroding surface. Semi-permeable layers can further affect the corrosion process by reacting with products and/or reactants. Reactions in semi-permeable layers include redox processes involving electron transfer, adsorption, ion-exchange and complexation reactions and precipitation/dissolution processes. Examples of porous and semi-permeable layers include non-reactive salt films, precipitate layers consisting of redox-active species in multiple oxidation states (e.g., Fe oxide films), clay and soil layers and biofilms. Examples of these various types of processes will be discussed and modelling techniques developed from studies for the disposal of high-level nuclear waste presented.

AECL
Whiteshell Laboratories
Pinawa, Manitoba R0E 1L0
1996

AECL-11592
COG-96-273

AECL EACL

MODÉLISATION DES EFFETS DES COUCHES POREUSES ET SEMI-PERMÉABLES SUR LES PROCESSUS DE CORROSION

par

F. King, M. Kolář et D.W. Shoesmith

RÉSUMÉ

Les couches poreuses et semi-perméables influent sur de nombreux processus de corrosion. Les couches poreuses peuvent influer simplement sur la vitesse de corrosion en influent sur la vitesse de transport de masse des réactifs et des produits en provenance de la surface subissant la corrosion et vers celle-ci. Les couches semi-perméables peuvent de plus influer sur le processus de corrosion en réagissant avec les produits ou les réactifs. Les réactions dans les couches semi-perméables comprennent les processus redox faisant intervenir des réactions de formation de complexes, d'échange d'ions, d'adsorption ou de transfert d'électrons, ainsi que les processus de précipitation-dissolution. Les minces couches de sel non réactives, les couches de précipité contenant des espèces redox-actives à différents stades d'oxydation (par ex. couches d'oxyde ferreux), les couches d'argile et de sol et les films biologiques sont des exemples de couches poreuses ou semi-perméables. On examine des exemples de ces divers types de processus et on présente des résultats d'études réalisées sur le stockage permanent des déchets nucléaires de haute activité.

EACL
Laboratoires de Whiteshell
Pinawa (Manitoba) R0E 1L0
1996

AECL-11592
COG-96-273

CONTENTS

1. INTRODUCTION

Mass transport through porous media and adsorption, precipitation/dissolution and redox reactions are important in many geochemical processes. The geochemical and soils literature contain numerous studies of these processes, many of which are relevant to corroding systems. The aim of this report is to review the mechanistic and empirical models developed by geochemists and soil scientists to describe these processes, and to show how they can be used in models to predict the corrosion behaviour of various materials. The corrosion of Cu nuclear fuel waste containers will be used as an example.

The use of engineered and natural barriers is a common method for preventing, or at least delaying, the transport of toxic wastes to the biosphere. This multi-barrier concept is currently being applied to the disposal of high-level radioactive waste in a number of countries. In Canada, the concept for the disposal of used nuclear fuel involves placing the fuel in a corrosion-resistant container, emplacing the container in an excavated vault deep underground and sealing the vault with various clay-based materials (AECL 1994, Figure 1). In this case, the various barriers (from the container surface outwards) include: a layer of sand, compacted buffer and backfill materials and the rock itself. All of these layers are porous and react with radionuclides released from the container, either through adsorption or precipitation processes or by redox reactions. These processes also affect the corrosion behaviour of the container.

The buffer and backfill materials consist of a compacted mixture of clay and aggregate (Johnson et al. 1994a). Buffer material is a 50:50 mixture (by dry mass) of Avonlea bentonite and silica sand. Backfill material consists of 70% crushed granite, 25% glacial-lake clay and 5% Avonlea bentonite. These mixtures will be compacted to target dry densities of ~1.65 $g \cdot cm^{-3}$ (buffer) and ~2.1 $g \cdot cm^{-3}$ (backfill), with porosities of ~0.4 and ~0.2, respectively. The hydraulic conductivity of these materials is sufficiently low ($<10^{-10}$ $m \cdot s^{-1}$) that mass transport will occur principally by diffusion.

Clay minerals are highly surface active materials because of their high specific surface area (~600 $m^2 \cdot g^{-1}$ for bentonite) and their ability to sorb cations (cation exchange capacity 60-80 meq/100 g for bentonite, Johnson et al. 1994a). Sorption involves both ion-exchange processes and adsorption at specific edge sites on the clay particles. The exchangeable cations (Na^+ in the case of Na-bentonite) balance the net negative surface charge caused by the substitution of divalent cations for Al^{3+} in the octahedral alumina layer of the 2:1 silica:alumina clay structure. Thus, adsorption and precipitation reactions will occur within the porous medium.

In addition, the buffer and backfill materials and granitic rock contain a number of redox-active species. For instance, the crushed granite in the backfill material mainly consists of quartz, plagioclase (Ca/Na feldspar) and K-feldspar, but also contains smaller amounts (0.1-5 wt.%) of Fe(II) containing minerals such as biotite, pyrite and magnetite. Clays also contain a number of oxidizable impurities, such as organic C, Fe_3O_4 and metallic Fe (Oscarson and Dixon 1989). These species will participate in redox reactions with O_2 and dissolved metal ions within the vault and geosphere.

2. FACTORS AFFECTING CORROSION REACTIONS IN POROUS AND SEMI-PERMEABLE LAYERS

The 1-D mass-balance equation for advective and diffusive mass transport is (Cook 1988; Stumm 1992)

$$\varepsilon_a \frac{\partial c}{\partial t} = \frac{\partial}{\partial x}\left(\tau \varepsilon_e D_0 \frac{\partial c}{\partial x}\right) - \varepsilon_a v \frac{\partial c}{\partial x} - \rho \frac{\partial s}{\partial t} + \rho \frac{\partial}{\partial x}\left(D_s \frac{\partial s}{\partial x}\right) + \varepsilon_a \sum R \qquad (1)$$

where c and s are the pore-water and adsorbed concentrations respectively, D_o and D_s are the pore-water and pore-surface diffusion coefficients (in the presence of flow, D_o is the dispersion coefficient, Stumm 1992), ε represents porosity, τ the tortuosity factor, ρ the dry density of the porous medium, v is the water velocity and R represents the rate of various reactions in the porous medium. Thus, the first term on the

right-hand side represents diffusion through the pores of the porous medium, the second term represents advective flow, the third term describes the net rate of adsorption and desorption, the fourth term describes surface diffusion of adsorbed species and the final term includes effects due to redox and complexation reactions and precipitation/dissolution processes. As described below, diffusion only occurs through a fraction of the total porosity (the effective porosity ε_e), whereas the various reactions can occur throughout the accessible porosity (ε_a).

Here, we shall be concerned with systems in which diffusive mass transport dominates, so the advective flow term can be ignored. Furthermore, if τ, ε, ρ, D_0 and D_s are independent of x, replacing $\partial s/\partial t$ with $(\partial s/\partial c)(\partial c/\partial t)$ and $\partial s/\partial x$ with $(\partial s/\partial c)(\partial c/\partial x)$ gives

$$\left(\varepsilon_a + \rho\frac{\partial s}{\partial c}\right)\frac{\partial c}{\partial t} = D_i\frac{\partial^2 c}{\partial x^2} + \varepsilon_a \sum R \qquad (2)$$

where D_i is the total intrinsic diffusion coefficient (See Equation (7), Cook 1988). The term $(\varepsilon_a + \rho(\partial s/\partial c))$ on the left-hand side of Equation (2) is called the capacity factor, and can be thought of as the porous and sorptive capacity of the medium for the solute. Alternatively, this term can be expressed as the retardation factor $(1 + (\rho/\varepsilon_a)(\partial s/\partial c))$, which represents the retardation of the diffusive transport of the solute due to the porous and sorptive nature of the medium (Stumm 1992).

2.1 DIFFUSION THROUGH POROUS MEDIA

2.1.1 Porosity, Tortuosity and Constrictivity

A number of different types of porosity have been defined to describe the porous nature of the compacted clay-sand buffer material in which nuclear waste containers will be emplaced (Figure 2). The total porosity ε is divided into accessible (ε_a) and non-accessible (ε_{na}) porosities (Oscarson et al. 1994)

$$\varepsilon = \varepsilon_a + \varepsilon_{na} \qquad (3)$$

The accessible porosity includes all connected through and dead-end pores, whereas the non-accessible porosity comprises isolated pores and inter-particle spaces that are physically too small for hydrated solutes to enter. In the case of compacted clay (which has a sheet-like structure), the inter-lamellar porosity is significant, and the non-accessible porosity may constitute up to 50% of the total (Oscarson et al. 1994). Since diffusing solutes cannot enter the non-accessible pores, the only solutes present within the isolated pores will be those trapped when the porous material is formed. Although these species may undergo some reactions within the isolated pores or inter-lamellar spaces, they have no influence on the corrosive environment and will not be considered further here.

In contrast, solutes and reactions occurring in the accessible porosity can influence the corrosive environment. The accessible porosity can be divided into an effective porosity for diffusive mass transport (ε_e) and a storage porosity (ε_s)

$$\varepsilon_a = \varepsilon_e + \varepsilon_s \qquad (4)$$

The effective and storage porosities are associated with the connected through-pores and the dead-end (or blind) pores, respectively. Solutes diffuse into and out of the accessible pores and undergo adsorption, precipitation, redox, complexation and other reactions within them. Any or all of these processes may influence the corrosion reaction. (Some authors consider ε_a and ε_e to be equal).

The network of through pores is further characterized by a tortuosity factor and the constrictivity. The tortuosity factor is defined by (Oscarson et al. 1992)

$$\tau = (L/L_e)^2 \tag{5}$$

where L is the straight-line distance between two points and L_e is the effective distance travelled by a diffusing species. As measured (see below), τ usually includes other factors, such as the variation in the pore diameter (the constrictivity), the variation in the solution viscosity in the pores and the effect of any excluded region of the pore space due, for instance, to repulsion between a diffusing anion and a negatively charged surface (Oscarson et al. 1992).

2.1.2 Diffusion Coefficients

Various diffusion coefficients can be used to describe diffusion through porous media. If there is no adsorption of the solute, the effective diffusion coefficient in the porous medium D_e is related to the diffusion coefficient in bulk solution D_o by (Cho et al. 1993)

$$D_e = \varepsilon_e \tau D_o \tag{6}$$

For adsorbed species, it is also necessary to consider surface diffusion. For clay-type materials, surface diffusion refers to the migration within the electrical double layer next to the mineral surface (Oscarson 1994). This form of diffusion is feasible for those solutes adsorbed at ion-exchange sites created by the net negative surface charge, but is not feasible for species specifically adsorbed at edge sites on the clay particles, which are bound more strongly. The total intrinsic diffusion coefficient includes both pore-water and surface diffusion terms and is defined by (Cook 1988)

$$D_i = \tau \varepsilon_e D_0 + \rho D_s \frac{\partial s}{\partial c} \tag{7}$$

Oscarson (1994), however, has shown that surface diffusion is not significant for the diffusion of Sr^{2+}, Ca^{2+} and Na^+ in compacted clays, at least to a clay density of 1.60 $g \cdot cm^{-3}$. In that case, $D_e = D_i$. Whether surface diffusion is important for other adsorbates and adsorbents will depend on the strength of the adsorbate-adsorbent interaction and on the nature of the adsorption sites. An apparent diffusion coefficient D_a can also be defined (Cook 1988; Cho et al. 1993)

$$D_a = \frac{D_i}{\varepsilon_a + \rho(\partial s / \partial c)} \tag{8}$$

In the absence of any reactions other than adsorption, Equations (2) and (8) give

$$\frac{\partial c}{\partial t} = D_a \frac{\partial^2 c}{\partial x^2} \tag{9}$$

The various diffusion coefficients and porosities defined above can be determined from experimental measurements. The ratio of the accessible to the total porosity ($\varepsilon_a/\varepsilon$) can be determined from equilibrium adsorption measurements on unconsolidated and compacted clay (Oscarson et al. 1994). In unconsolidated clay, the solute has access to all of the adsorption sites, whereas in compacted media only those sites accessible to the solutes will be occupied. On the assumption that the number of adsorption sites is proportional to the porosity, the ratio of the concentration of adsorbed species on the compacted clay to that on the unconsolidated clay equals $\varepsilon_a/\varepsilon$. The total porosity ε can be calculated from the density of the compacted medium and the specific gravity of the clay (Craig 1987).

The effective diffusion coefficient ($\tau\varepsilon_e D_o$) can be determined from steady-state diffusion experiments (Oscarson et al. 1992). For non-sorbing species (i.e., $\partial s/\partial c = 0$), diffusion coefficients measured under

transient conditions give a value for τD_o (on the assumption $\varepsilon_a = \varepsilon_e$) so that a combination of the two experiments gives values for τ and ε_e (assuming D_o is known). For the reference compacted buffer material proposed for a Canadian nuclear waste disposal vault, $\tau \approx 0.1$, $\varepsilon \approx 0.4$, $\varepsilon_a \approx \varepsilon_{na} \approx 0.2$ and $\varepsilon_e \approx \varepsilon_s \approx 0.1$ (Oscarson et al. 1992, 1994).

2.1.3 Diffusion in Unsaturated Porous Media

An additional complication arises if the porous material is only partly saturated with solution, and some of the pores are filled by gas or vapour. Then, particularly if one or more of the solutes is mobile in the gas phase, such as O_2, the effect of gas-filled porosity must be taken into account. Collin and Rasmuson (1988) have shown that the effective diffusion coefficient of a gas through unsaturated soils (D_{eff}) is a strong function of the degree of saturation S. For fully saturated soils (i.e., $S = 1.0$), $D_{eff} \sim 10^{-7}$ cm^2·s^{-1}, whilst at $S = 0.9$, D_{eff} can be up to three orders of magnitude higher because of enhanced diffusion in the gas phase.

Large pores tend to dry out before small pores because of the lower capillary pressure. As a consequence, D_{eff} is a complicated function of S (Collin and Rasmuson 1988). King and Kolář (1995) used a cubic relationship between S and D_{eff} to describe O_2 diffusion through unsaturated buffer material

$$D_{eff} = \tau_s \varepsilon_{es} D_o + \kappa_{eq} \tau_g (1-S)^3 \varepsilon_{eg} D_g \qquad (10)$$

where τ_s and τ_g are the tortuosity factors for the solution-filled and gas-filled pores, ε_{es} and ε_{eg} are the respective effective porosities, D_g is the gas-phase diffusion coefficient and κ_{eq} is related to the Henry's Law distribution coefficient of O_2 between the solution and gas phases.

Although the major effect of unsaturated conditions is on the diffusion coefficient of species that can partition into the gas phase, decreasing moisture content also has an effect on diffusion in solution. Conca and Wright (1991) found a relationship between D_e for a number of solutes and the volumetric water content for various types of soil. Between water contents of 20% and 0%, D_e decreased by up to three orders of magnitude, as the connectivity between solution-filled parts of the pore structure decreased. Thus, at very low moisture contents, there could be rapid diffusion of O_2 to the corroding surface, but slow rates of diffusion of dissolved species such as Cl^- or soluble corrosion products to and from the interface.

2.1.4 Effect of Porosity on Corrosion Reactions

An example of the effects of porous layers on corrosion reactions is the effect of various water-saturated layers on the corrosion of Cu in O_2-containing Cl^- solutions (King et al. 1995a). In this case, neither reactant (O_2) nor product ($CuCl_2^-$) is adsorbed, so the effects observed are due solely to the change in ε and τ. In bulk solution ($\varepsilon\tau = 1$), the anodic dissolution of Cu is transport limited at the corrosion potential (E_{CORR}) and the cathodic reduction of O_2 is interfacially controlled. Consequently, the steady-state E_{CORR} decreases, and i_{CORR} increases, with increasing rates of mass transport, achieved by increasing the rotation rate f of a rotating-disc electrode (RDE) (King et al. 1995a). When the rate of mass transport to and from the electrode is reduced by placing a porous nylon membrane ($\varepsilon\tau < 1$) over the surface of the RDE, E_{CORR} is independent of both f and the mean pore size of the membrane. This suggests that both reactions are controlled by the same rate-determining step (rds), possibly the respective diffusion processes across the nylon membrane (King 1987). When the rate of diffusion is reduced even further by placing a layer of compacted clay over the electrode ($\varepsilon\tau = 0.01$), both anodic and cathodic reactions become totally limited by diffusion across the porous layer. Consequently, the interfacial $[O_2] \sim 0$ and the steady-state E_{CORR} is independent of layer thickness (King et al. 1995a; King 1987). Thus, decreasing permeability of the diffusion layer causes increasing transport control of the anodic and cathodic reactions.

2.2 ADSORPTION AND DESORPTION

2.2.1 Adsorption Models

Adsorption models can be broadly classified as being either equilibrium or kinetic models. In the area of nuclear waste disposal, it is usually assumed, but infrequently demonstrated, that the rate of diffusion is slow compared to the rates of adsorption and desorption and that, therefore, equilibrium models are applicable. Here, both equilibrium and kinetic models are described. More detailed reviews of various adsorption models are given elsewhere (Travis 1978; Haworth 1990; Stumm 1992).

In most soils there is more than one type of adsorption site. For clays, sorption may occur on the faces of the clay layers due to the net negative charge on the clay particles. This negative charge is created by the isomorphic substitution of divalent cations (such as Fe^{2+} or Mg^{2+}) for trivalent Al^{3+} in the alumina lattice (Johnson et al. 1994a). The charge-balancing cations are readily exchanged. On the surfaces of non-substituted oxides, such as the various Fe oxides or $Al_2O_3 \cdot xH_2O$, adsorption may occur at specific sites (Stumm 1992). Site-specific adsorption, such as at edge sites corresponding to terminal oxygen atoms, can take the form of surface complexation, surface hydrolysis (if H^+ is the adsorbate), surface ligand exchange or hydrogen-bond formation (Stumm 1992). Although site-specific adsorption models provide detailed information about the adsorption process, they are generally difficult to include in coupled mass-transport/adsorption models, and will not be considered further here.

Equilibrium adsorption models have the advantage that the resultant mass-transport/adsorption equation can be solved analytically (Travis 1978). For instance, the adsorption of small amounts of radionuclides on mineral surfaces is often described by a linear, equilibrium isotherm (Johnson et al. 1994a)

$$K_d = s/c \tag{11}$$

where the distribution coefficient K_d is equal to the term $\partial s/\partial c$ in Equation (2). If the solute undergoes no reactions other than adsorption (i.e., $\sum R = 0$), Equation (2) is easily solved. The Freundlich isotherm ($s = Kc^n$, where K and n are constants) has also been widely used, but like the linear isotherm does not define a maximum surface coverage (Travis 1978). The Langmuir isotherm (Travis 1978; Haworth 1990; Stumm 1992)

$$s = \frac{K' s^{max} c}{1 + K' c} \tag{12}$$

does include a maximum surface coverage s^{max} (K' is a constant) and has been found to describe the adsorption of many solutes on soils (Travis 1978; Ryan and King 1994).

Many of these equilibrium isotherms have kinetic counterparts. Thus, the rate of change of the surface coverage for a kinetic linear model is given by (Travis 1978)

$$\frac{\partial s}{\partial t} = k \frac{\varepsilon}{\rho} c - k' s \tag{13}$$

where k and k' are rate constants for the adsorption and desorption steps, respectively. The equilibrium expression (Equation (11)) is obtained if $\partial s/\partial t = 0$ ($K_d = k\varepsilon/k'\rho$). The kinetic Freundlich model is virtually identical to Equation (13), except that the rate of adsorption is proportional to c^n. In the kinetic Langmuir model, the rates of adsorption and desorption are proportional to the concentrations of unoccupied and occupied sites, respectively

$$\frac{\partial s}{\partial t} = kc\left(s^{max} - s\right) - k' s \tag{14}$$

The kinetic Langmuir model has been less frequently used than the kinetic linear or Freundlich models because the resultant coupled mass-transport/adsorption equation cannot be solved analytically (Travis 1978). Another kinetic adsorption model is the Elovich model (Travis 1978; Stumm 1992)

$$\frac{\partial \Gamma}{\partial t} = k \exp(-k' \Gamma) \tag{15}$$

where $\Gamma = s/s^{max}$. The Elovich equation can be interpreted as representing an adsorption process for which the number of available sites decreases exponentially with s or where the heat of adsorption decreases linearly with the surface coverage.

The choice of whether to use an equilibrium or a kinetic adsorption expression depends (assuming an analytical solution to the advection-diffusion/adsorption equation is not required) on the relative rates of mass transport and adsorption/desorption. In flow-dominated systems, kinetic models may be more appropriate whereas, with the slower rates of mass transport in diffusion-dominated regimes, equilibrium models may be adequate. Koopman et al. (1992) derived a criterion to decide whether local equilibrium could be assumed for adsorption following a Langmuir-type adsorption process. Using the notation in Equation (14), local equilibrium is established if

$$t_r k' > A \tag{16}$$

where A is a constant with a value ~3-4 and t_r is the residence time of the solute within a given region. Thus, the condition of equilibrium depends on the rate of desorption, but not on the rate of adsorption. Equation (16) also indicates the size of the domain over which the condition of equilibrium can be assumed to apply. For Cu(II) desorption from bentonite clay, preliminary results suggest $k' \sim 10^{-6}$ s^{-1} at 25°C (King and Kolář 1995; King and Ryan, unpublished data). Therefore, for A = 3, equilibrium can only be assumed over a distance greater than that across which Cu(II) diffuses in ~35 d, of the order of a few mm. In comparison, the distance between adsorption sites on the clay particles is of the order of 1 nm (for a cation exchange capacity of 60 meq/100 g and a specific surface area of 600 $m^2 \cdot g^{-1}$ for bentonite clay, Johnson et al. 1994a). Therefore, the adsorption of Cu on a particular adsorption site cannot be considered to be at equilibrium.

An alternative method for deciding the relative importance of diffusion and the rate of reaction is based on the definition of a dimensionless parameter known as the Damköhler number (Wersin et al. 1994). Let us define a dimensionless parameter $z = x/l$, where l is a characteristic length. Then, in the absence of flow, surface diffusion and any reaction other than sorption, Equation (1) becomes

$$\varepsilon_a \frac{\partial c}{\partial t} = \frac{D_i}{l^2} \frac{\partial^2 c}{\partial z^2} - \rho \frac{\partial s}{\partial t} \tag{17}$$

If adsorption follows the Langmuir model (Equation (14)), the fastest net rate of adsorption is $kc(s^{max}-s)$. The Damköhler number (Da) is then given by

$$Da = \frac{\rho l^2 k (s^{max} - s)}{\varepsilon_a D_i} \tag{18}$$

For Da > 10, the reaction rate is significantly faster than diffusion and equilibrium can be assumed within the characteristic length l. The greatest rate of adsorption occurs when all the sorption sites are unoccupied (s = 0). For the adsorption of Cu(II) on compacted bentonite ($k = 2 \times 10^{-3}$ $dm^3 \cdot mol^{-1} \cdot s^{-1}$, $D_i = 10^{-7}$ $cm^2 \cdot s^{-1}$, $\varepsilon_a = 0.2$, $\rho = 1.65$ $kg \cdot dm^{-3}$, King and Kolář 1995; King and Ryan, unpublished data), equilibrium would be achieved for l > 0.4 mm, again much greater than the distance between neighbouring adsorption sites on the clay surface. With increasing rate of diffusion (i.e., higher T, higher ε) and/or

greater surface coverage (i.e., lower net rate of adsorption), I increases. Thus, although equilibrium can be assumed on a macroscopic scale, locally the adsorption process cannot be described by an equilibrium isotherm because the rate of adsorption is not fast compared with the rate of diffusion.

2.2.2 Effect of Adsorption on Corrosion Reactions

Adsorption lowers the activity of dissolved species in the pore solution, and may increase the corrosion rate of metals undergoing reversible dissolution

$$M \rightleftharpoons M^{n+} + ne^- \rightleftharpoons MY^{(n-m)+} \tag{19}$$

where Y^{m-} represents an adsorption site. This effect has been used to explain the effect of the dissolved Cu speciation on the corrosion rate of Cu in O_2-containing Cl^- solutions in the presence of compacted buffer material (King et al. 1992). Under conditions in which Cu dissolved primarily as Cu(II), relatively high corrosion rates and high $[Cu]_{ads}$ were observed. When Cu dissolved as Cu(I) (stabilized as anionic $CuCl_2^-$ complexes), however, low corrosion rates and low $[Cu]_{ads}$ were found. Thus, the adsorption of Cu(II) cations (either as Cu^{2+}, $CuCl^+$ or $Cu(OH)^+$) reduced the dissolved [Cu], resulting in higher corrosion rates and higher $[Cu]_{ads}$. Conversely, when $CuCl_2^-$ species (which are not adsorbed by the negatively charged adsorption sites on the clay particles) were formed, adsorption did not drive the dissolution reaction.

Adsorption may also affect the formation of aggressive environments within porous media. Within oxide-filled pits, crevices or cracks, for instance, the oxide may, depending upon the bulk pH compared with pH_{pzc}, either adsorb cations (thus suppressing local acidification due to hydrolysis) or anions (preventing an increase in the [Cl], for example, within the occluded region). Although the adsorbed species would generally be benign from a corrosion viewpoint, adsorption does lead to concentration of these potentially aggressive species which, if conditions change, could be released resulting in accelerated corrosion. It is not only solute species that may be adsorbed. Hygroscopic porous media may reduce the water activity (a_w) by adsorbing water from the pore solution. This could either serve to concentrate the solutes making them more aggressive or have the opposite effect by lowering a_w to such an extent that the metal surface in contact with the porous medium is devoid of sufficient surface water to support aqueous electrochemical reactions.

2.3 PRECIPITATION AND DISSOLUTION REACTIONS

2.3.1 Precipitation

Even if a corroding surface is not initially in contact with a porous layer, such an environment could develop due to the precipitation of corrosion products. Precipitation and dissolution reactions play a key role in geochemical processes and have been extensively studied. Precipitation can be divided into nucleation and growth processes. In both cases, the degree of supersaturation of the solution (θ) is important (Stumm 1992)

$$\theta = a/a_0 \tag{20}$$

where a is the activity of the solute in solution and a_0 is the activity in a saturated solution in equilibrium with the solid phase.

Nucleation can occur in solution (homogeneous) or on a surface (heterogeneous). The free energy change upon nucleation is a balance between the energy gained by the formation of bonds between the species in the nucleus and the work required to form the surface. For a spherical nucleus of radius r, the free energy change for nucleation is given by (Stumm 1992)

$$\Delta G = -jkT \ln\theta + 4\pi r^2\gamma \quad (21)$$

where j is the number of molecular units in the nucleus, k is Boltzmann's constant and γ is the interfacial energy. The free energy, and hence the rate of nucleation, is critically dependent upon the degree of supersaturation.

Surfaces catalyze the nucleation process by decreasing the work required for the creation of the new surface (the second term on the right-hand side of Equation (21), Stumm 1992). The most catalytic type of surface is one for which there is a good match between the substrate structure and that of the precipitating solid (epitaxial growth). Then the work required to create the new precipitate/solution interface is equal to that gained from the loss of the substrate/solution interface. Precipitation in this case tends to be 2-dimensional. If the surface energy of the substrate/solution interface is greater than that of the precipitate/solution interface, growth of the precipitate will tend to occur on the existing precipitate surface, leading to 3-dimensional growth. Surfaces can also catalyze nucleation by increasing the frequency of collisions between solutes through their adsorption on the surface (Stumm 1992). Although the activation energy for nucleation can be used to give a kinetic expression for the rate of nucleation, the various interfacial energy terms are, unfortunately, not known very accurately. In general, however, heterogeneous nucleation lowers the degree of supersaturation required for nucleation. In corroding systems, precipitation occurs close to the corroding surface because the degree of supersaturation is highest at that location.

Empirical growth laws also involve the degree of supersaturation. Two rate laws commonly used to describe precipitation growth kinetics are (Stumm 1992)

$$V = k(\theta-1)^n \quad (22)$$

$$V = A(\ln\theta)^m \quad (23)$$

where V is the linear growth rate ($m \cdot s^{-1}$), k and A are rate constants and n and m are empirical constants. For Equation (22), n is commonly ~2 (Stumm 1992). Equation (23) can also be used to predict the rate of dissolution if $\theta<1$.

2.3.2 Dissolution

The dissolution (or weathering) of minerals is very important in geochemistry. A number of possible rds can be identified, including: the transport of reactants to the surface, adsorption, chemical, diffusion or redox processes occurring on the surface, desorption or detachment reactions and mass transport in solution away from the precipitate surface. In general, any of these steps could be rate controlling. Dissolution reactions are classified as being either diffusion-controlled or surface-controlled processes (Stumm 1992).

Dissolution could be diffusion controlled either by diffusion in solution or because of diffusion of a reactant or product across a surface layer. Solution-transport controlled dissolution processes are relatively uncommon, and require either a very fast interfacial step(s) or a very slow rate of diffusion. In these cases, the solute concentration at the dissolving interface can be assumed to be at equilibrium with the solid phase, since the preceding interfacial steps must be fast compared with the rate of diffusion. A possible example of a transport-limited dissolution reaction is the dissolution of used fuel under anoxic conditions in a nuclear waste disposal vault (Johnson 1994b). Here, the rate of dissolution of the (mainly) UO_2 matrix, and of the congruent release of radionuclides dissolved and trapped in the UO_2 matrix, can be calculated based on equilibrium solubility predictions coupled to a diffusive mass-transport equation (Johnson 1994b).

An example of a dissolution process limited by diffusion across a surface layer is the dissolution of biotite (of the general form $K(Mg_{0.6\text{-}1.8}Fe^{II}_{2.4\text{-}1.2})(Si_3Al)O_{10}(OH,F)_2$). The release rate of Fe(II) is found to decrease

with time as a surface layer depleted in Fe(II) is formed (Malmström et al. 1995). This transient period is then followed by a steady-state period, during which the surface layer thickness is constant. In the steady state, the dissolution rates of all elements are the same, and are equal to the dissolution rate of the least soluble species. The rate of dissolution, expressed as the release rate of Fe(II), is given by (Kolář and King 1996)

$$d[Fe(II)_{aq}]/dt = A[R_0 e^{-\beta t} + R_1] \quad (24)$$

where A is the surface area, R_0 and R_1 are the instantaneous and steady-state Fe(II) dissolution rates and β is a constant dependent upon the length of time to reach steady state.

Dissolution reactions controlled by the diffusion of species across a surface layer are, in the steady state, surface-controlled processes (Stumm 1992). In general, surface-controlled dissolution rates are given by

$$\text{rate} = kA[\text{reactant}] \quad (25)$$

where k is a rate constant and A is the surface area. The reaction order with respect to the concentration of various reactants (e.g., H^+, Cl^-) can be determined empirically, from which the rate expression and identity of the rds can be deduced. The rate of surface-controlled dissolution reactions is often enhanced by surface complexation or surface protonation (Stumm 1992). In some cases, such as the oxidative dissolution of UO_2 (Shoesmith and Sunder 1992) or the reductive dissolution of Fe_3O_4 (Mancey et al. 1993), dissolution is accompanied by a change in oxidation state of the substrate. In these cases, the rate of dissolution is potential-dependent, so that the potential of the dissolving surface must be known in order to predict the rate of dissolution.

2.3.3 Effects of Precipitation on Corrosion Reactions

Precipitation can have a number of effects on corrosion reactions. As with adsorption, precipitation may increase the dissolution rate of diffusion-controlled reactions (for which the preceding dissolution step(s) are reversible) by lowering the activity of the dissolved species (Equation (19)). The degree of enhancement of the dissolution rate is greatest when precipitation occurs close to the point of dissolution, thus maintaining a steep concentration gradient (Garisto and Garisto 1986). Such effects have been included in the model for the dissolution of used fuel under anoxic conditions in a Canadian disposal vault (Johnson et al. 1994b). Alternatively, the formation of a precipitate layer can inhibit corrosion by acting as a mass-transport barrier to continued dissolution. The quality of the film may vary from a highly protective passive layer to a less-protective defected, porous layer. In turn, redox reactions and adsorption processes may occur within the precipitated layer. These reactions within the growing film could be modelled using similar expressions to those used to describe these processes in porous media such as soils or compacted buffer material. Finally, precipitate layers may either catalyze or inhibit the rate of electron-transfer reactions. For instance, the rate of reduction of O_2 on Cu_2O is lower than the rate of reduction on "bare" Cu. This phenomenon is believed to account for the good corrosion resistance of Cu alloys in natural waters (Kato et al. 1980a,b).

2.4 REDOX REACTIONS

2.4.1 Nature of Redox Reactions in Soils

Most geological environments contain redox-active species. The consumption of O_2, the cycling of Fe in the environment and the oxidation and reduction of dissolved metal ions are common examples of such reactions (Stumm 1992). These reactions occur either in solution (homogeneous) or on the surfaces of electrically-conducting particles (heterogeneous). The modelling of homogeneous redox processes is generally simpler than that for heterogeneous reactions. For example, the homogeneous oxidation of Cu(I)

or Fe(II) by O_2

$$4Cu(I) + O_2 + 2H_2O \rightarrow 4Cu(II) + 4OH^- \quad (26)$$

$$4Fe(II)_{aq} + O_2 + 2H_2O \rightarrow 4Fe(III)_{aq} + 4OH^- \quad (27)$$

can be described by the simple kinetic expressions (Sharma and Millero 1988; Stumm 1992)

$$-d[Cu(I)]/dt = k[O_2][Cu(I)] - k'[Cu(II)] \quad (28)$$

$$-d[Fe(II)]/dt = k[O_2][Fe(II)][OH^-]^2 \qquad pH > 5 \quad (29)$$

These expressions are then substituted for the reaction rate term in Equation (1). Similarly, if oxidation involves adsorbed Fe(II) species, the concentration of these species can be substituted for [Fe(II)] in Equation (29)

$$-d[Fe(II)]/dt = k\langle Fe(OM\equiv)_2\rangle[O_2] \quad (30)$$

where $\langle Fe(OM\equiv)_2\rangle$ represents the concentration of Fe(II) adsorbed, for example, on surface hydroxyl groups of a hydrous oxide (Stumm 1992).

For redox reactions occurring on surfaces, however, it is more appropriate to treat the reacting surface as an electrochemical interface. Then, on the assumption that the surface supports both anodic and cathodic reactions, the rate of reaction can be determined by coupling together electrochemical expressions describing the rates of the two (or more) processes. This is the basis of mixed-potential models, which have been applied to corroding surfaces in porous media (King and Kolář 1995; King et al. 1995a). If the surface on which the redox reactions are occurring is the corroding surface, then it is most convenient to use the electrochemical expressions as boundary conditions for the solution of mass-balance equations such as Equation (1). If the only anodic reaction considered is the metal dissolution reaction, then the potential predicted is E_{CORR} (Macdonald and Urquidi-Macdonald 1990). If the anodic dissolution reaction is excluded, then the potential predicted is the redox potential (Macdonald and Urquidi-Macdonald 1990) (referred to as E_h in the geochemical literature, Stumm 1992).

Mixed-potential models can also be applied to redox reactions occurring on surfaces other than the corroding surface. For instance, the oxidation of pyrite (FeS_2) follows the overall reaction (Williamson and Rimstidt 1994)

$$FeS_2 + 7/2O_2 + H_2O \rightarrow Fe^{2+} + 2SO_4^{2-} + 2H^+ \quad (31)$$

This reaction is a multistep electrochemical process occurring on the semi-conducting pyrite surface, and nominally involves the oxidation of S and the reduction of O_2. Ferric ions are intermediate species, at least in acidic solution, as indicated by the dependence of the rate on [Fe(III)] (Williamson and Rimstidt 1990). Provided the electrochemical expressions for the individual anodic and cathodic reactions are known, the rate of pyrite oxidation (or of O_2 reduction) can be calculated as a corrosion current density i_{CORR}. This i_{CORR} term can then be expressed as a flux using Faraday's law and directly substituted in the reaction term of Equation (1), along with the area of exposed pyrite per unit volume. The pyrite surface area may vary with time, especially if the amount of pyrite is small compared with the amount of available O_2. In such cases, the decrease in pyrite surface area as the reaction proceeds can be compensated for using "shrinking-core" models or other geometrical corrections that account for the proportional decrease in surface area with decreasing dimension of the particles (Werme et al. 1992).

2.4.2 Effect of Redox Reactions on Corrosion Processes

One way in which redox reactions will affect corrosion processes is by changing the environment. For instance, Reactions (26) and (27) result in the consumption of O_2 and the formation of Cu(II) and Fe(III) species. If the amount of O_2 is limited then the extent of corrosion will be reduced (Kolář and King 1996). Furthermore, depending upon the composition of the solution, the oxidized metal ions may react further via adsorption, precipitation or redox reactions.

A second way in which redox reactions will affect corrosion reactions is by participating in interfacial reactions at the corroding surface. The interfacial reduction of oxidants may increase the rate of metal dissolution, whereas the oxidation of reduced species on the surface may decrease the rate of corrosion. The oxidative or reductive dissolution of protective corrosion-product layers will also affect the corrosion behaviour of the substrate.

3. A MODEL FOR THE CORROSION OF COPPER NUCLEAR WASTE CONTAINERS

A model has been developed to describe the corrosion behaviour of Cu containers in the conceptual disposal vault described in the introduction. Most of the processes described above are included in the model. Figure 3 shows the mechanism for the uniform corrosion of Cu in O_2-containing Cl^- solutions derived from the results of electrochemical studies and from corrosion experiments under simulated disposal conditions (King and Kolář 1995).

3.1 DESCRIPTION OF THE MODEL

The model consists of six mass-balance equations similar to Equation (1), which describe the mass-transport, adsorption/desorption, precipitation/dissolution and redox reactions of six of the species involved in the corrosion mechanism. The six species considered are: O_2, dissolved Cu(I) (as $CuCl_2^-$), precipitated Cu(I) (as Cu_2O), dissolved Cu(II) (as Cu^{2+}), precipitated Cu(II) (as $CuCl_2 \cdot 3Cu(OH)_2$), and Cu(II) adsorbed on bentonite. Dissolved and gas-phase O_2 are assumed to be in equilibrium, with the relative distribution given by Henry's law. All other reactions are described by kinetic expressions. Kinetic models are used instead of equilibrium models because, despite the slow rates of mass transport in compacted buffer and backfill materials, the rates of certain processes (e.g., Cu(II) adsorption and desorption on bentonite, the dissolution of Cu_2O and $CuCl_2 \cdot 3Cu(OH)_2$) may be sufficiently slow that local equilibrium is not established. Of all the reactions studied, the only one for which we have experimental evidence indicating that the rate is sufficiently fast that equilibrium can be assumed is the anodic dissolution of Cu in Cl^- solutions. Nevertheless, we treat all reactions, including the anodic dissolution of Cu, using kinetic expressions.

As an example, the mass-balance equation for Cu^{2+} (concentration c_2^s) is

$$\varepsilon_a \frac{\partial c_2^s}{\partial t} = \tau \varepsilon_e D_2 \frac{\partial^2 c_2^s}{\partial x^2} + \varepsilon_a \left[k_7 c_0^s c_1^s - \left(k_{-7} + k_8 c_3^s \right) c_2^s \right] - \varepsilon_a k_9 \max\left(0, c_2^s - c_2^{sat}\right) + 4k_{-9} c_2^p - k_{11} \varepsilon_a c_2^s \left(s_2^{max} - s_2 \right) \rho + k_{-11} s_2 \rho \qquad (32)$$

where c_0^s, c_1^s, c_2^p, s_2 and c_3^s are the concentrations of dissolved O_2, $CuCl_2^-$, $CuCl_2 \cdot 3Cu(OH)_2$, adsorbed Cu(II) and Fe(II) respectively, s_2^{max} is the maximum surface coverage of Cu(II) on bentonite, D_2 is the diffusion coefficient of Cu^{2+} in solution, and the various rate constants k are defined in Figure 3. The six mass-balance equations are solved using finite difference techniques. Although diffusion through any number of layers can be included in the model, in this version the disposal vault is simulated by a 1-m-thick layer of buffer material in contact with a 50-m-thick layer of rock. The right-hand edge of the rock (x = 51 m)

represents a major groundwater-bearing fracture in the rock , with a constant $[O_2]$ of 3.1 x 10^{-7} mol·dm^{-3} (10 ng·g^{-1}). Zero-concentration boundary conditions (bc) are used for the five Cu species at x = 51 m. At x=0, zero-flux bc are used for Cu_2O, Cu^{2+}, $CuCl_2 \cdot 3Cu(OH)_2$ and adsorbed Cu(II). The interfacial bc for O_2 and $CuCl_2^-$ are described below. The characteristics of the finite-difference grid and time increments are described by King and Kolář (1995), except that a non-equidistant grid generated by a geometric progression was used as described by Kolář and King (1996).

3.1.1 Diffusion Through Porous Media

The treatment of diffusion through the layer of compacted buffer material is the same as that described in the previous section (compare Equations (1) and (32)). Diffusion occurs through a medium of effective porosity ε_e and tortuosity factor τ. Surface diffusion of adsorbed species is not considered, neither is convective flow. For unsaturated buffer, the effective diffusion coefficient of O_2 is given by Equation (10). The effective porosity for species diffusing only in the solution phase is taken to be proportional to S, varying linearly from 0 at S=0 to the maximum value of 0.1 at S=1 (Figure 4).

3.1.2 Adsorption and Desorption

Equilibrium adsorption measurements of Cu(II) on Na-bentonite show that adsorption follows a Langmuir isotherm (Ryan and King 1994). Because of the uncertainty over the establishment of local equilibrium, however, a kinetic model is used to describe the effects of adsorption and desorption on the mass transport of Cu(II). Thus, the net rate of adsorption is given by

$$\partial s_2/\partial t = k_{11}\varepsilon_a c_2^s(s_2^{max}-s_2)\rho - k_{-11}s_2\rho \qquad (33)$$

(cf. Equation (14)). The negatively charged $CuCl_2^-$ species and neutral dissolved and gaseous O_2 molecules are assumed not to adsorb. Adsorption of dissolved Fe(II) is not considered either.

3.1.3 Precipitation and Dissolution Reactions

Relatively little is known about the mechanisms or rates of precipitation and dissolution of Cu_2O and $CuCl_2 \cdot 3Cu(OH)_2$. The little experimental evidence available suggests that Cu_2O forms from the hydrolysis of $CuCl_2^-$ (k_5, Figure 3), rather than the hydrolysis of a CuCl layer (k_6, Figure 3) or the dehydration of $Cu(OH)_{ads}$ (k_4, Figure 3, King 1996). Preliminary studies (Légère and King, unpublished data) on the dissolution of Cu_2O powder in Cl^- solutions (k_{-5}, Figure 3) suggest that the rate is proportional to $[H^+]$ but relatively insensitive to $[Cl^-]$ and has an activation energy of ~35 kJ·mol^{-1}. The mechanism and rate of dissolution may be different for Cu_2O films on Cu surfaces. No information is available regarding the precipitation or dissolution of $CuCl_2 \cdot 3Cu(OH)_2$.

In the model, we assume that the rate of nucleation is fast and that the rds is the growth of the precipitated phase. This is probably a reasonable assumption given the large surface area:volume ratio in buffer material because of the presence of surface-active clay minerals and other surfaces. Heterogeneous nucleation will be catalyzed by the lower interfacial energy required for nucleus formation (Equation (21)) and, in the case of Cu(II), by the increased frequency of interactions of adsorbed Cu(II) species. The rate of precipitation is assumed to be proportional to the degree of supersaturation. For example, the rate of precipitation of $CuCl_2 \cdot 3Cu(OH)_2$ is given by (see Equation (32))

$$\text{rate of } CuCl_2 \cdot 3Cu(OH)_2 \text{ precipitation} = \varepsilon_a k_9 \max(0, c_2^s - c_2^{sat}) \qquad (34)$$

where the $\max(0, c_2^s - c_2^{sat})$ term ensures that precipitation does not occur from undersaturated solutions. Equation (34) is equivalent to Equation (22) with n=1, but predicts precipitation on a volume basis rather than in terms of a linear growth rate. Equation (34) predicts that precipitation will occur for θ>1. This

degree of supersaturation is lower than that required for the precipitation of other solids (Stumm 1992), but was chosen here because of the lack of other information and because of the high surface area:volume ratio in this system.

The rate of dissolution is assumed to be proportional to the concentration of the precipitated solid (expressed on a bulk volume basis). Thus, the rate of dissolution of $CuCl_2 \cdot 3Cu(OH)_2$ is simply given by

$$\text{rate of } CuCl_2 \cdot 3Cu(OH)_2 \text{ dissolution} = k_{-9} c_2^p \tag{35}$$

The rate constant k_{-9} implicitly contains terms for the dependence of the dissolution rate on, for example, pH, $[Cl^-]$, $[Cu^{2+}]$, etc. Furthermore, since dissolution experiments give the dissolution rate per unit area, the molar surface area of the precipitated solid must also be estimated. The molar surface area will depend on the size and morphology of the deposits, and can only be estimated from experimental observation.

3.1.4 Redox Reactions

Two types of redox reaction are included in the model; interfacial anodic and cathodic reactions and homogeneous redox reactions involving O_2, $CuCl_2^-$, Cu^{2+} and Fe(II). The interfacial electrochemical reactions are used as flux bc for O_2 and $CuCl_2^-$ at x=0. The anodic current density (i_a) for the dissolution of Cu in chloride solutions (rate constants k_1/k_{-1} and k_2/k_{-2} in Figure 3) is (King and Kolář 1995)

$$i_a/n_aF = (k_1k_2/k_{-1})[Cl^-]^2 \exp[F/RT(E - E_a^o)] - k_{-2}[CuCl_2^-]_o \tag{36}$$

where n_a is the number of electrons transferred per copper atom ($n_a = 1$), E_a^o is the standard potential and $[CuCl_2^-]_o$ is the interfacial concentration of $CuCl_2^-$. The cathodic current density (i_c) for the reduction of O_2 is (King and Kolář 1995)

$$-i_c = n_cFk_c^o[O_2]_o \exp[-\alpha_cF/RT(E - E_c^o)] \tag{37}$$

where n_c is the number of electrons transferred per O_2 molecule ($n_c = 4$), k_c^o is the standard rate constant for O_2 reduction to OH^-, $[O_2]_o$ is the interfacial dissolved oxygen concentration, α_c is the cathodic transfer coefficient and E_c^o is the standard potential for the 4-electron reduction of O_2 to OH^- (experimental evidence shows that the 2-electron reduction of O_2 to HO_2^-, rate constant k_b in Figure 3, is not significant for Cu under these conditions, Vazquez et al. 1994; King et al. 1995b,c). Equations (36) and (37) are linked by expressions for the interfacial fluxes of $CuCl_2^-$ and O_2, namely

$$i_a = n_aF\tau\varepsilon_e D_1 \frac{\partial c_1^s(0,t)}{\partial x} \tag{38}$$

and

$$-i_c = n_cFD_{eff} \frac{\partial c_0^s(0,t)}{\partial x} \tag{39}$$

respectively, where D_1 is the bulk solution diffusion coefficient of $CuCl_2^-$.

On the assumption that the anodic and cathodic reactions can occur anywhere on the surface, $i_a = -i_c = i_{CORR}$ at $E = E_{CORR}$. Combining Equations (36)-(39) gives bc for O_2 and $CuCl_2^-$ in terms of i_{CORR}. This is the basis of mixed-potential models which, as well as providing the corrosion rate (in terms of i_{CORR}), also give a value for E_{CORR} by substituting i_{CORR} in either Equation (36) or (37) (King and Kolář 1995; King et al. 1995a).

The possibility for the interfacial reduction of Cu^{2+} is also included in the model (rate constant k_{10}, Figure 3). Although this reaction can occur on bare Cu surfaces (Peters and Cruser 1965), it is unlikely to proceed on surfaces covered by an electrically insulating layer of $CuCl_2 \cdot 3Cu(OH)_2$. Predictions from the model suggest the precipitation of $CuCl_2 \cdot 3Cu(OH)_2$ is likely to occur, so this interfacial reaction is not included in the calculations below.

Homogeneous redox reactions involving the oxidation of $CuCl_2^-$ and Fe(II) by O_2 (Reactions (26) and (27)) are included in the model. These reactions are described by the respective rate expressions (Equations (28) and (29)), except that the $[OH^-]^2$ term is included in the value of the rate constant for the reaction between Fe(II) and O_2 (pH 7 is assumed). The concentrations of $CuCl_2^-$ and O_2 are functions of x and t, as described by the mass-balance equations, so that the rate of the oxidation reactions also varies in space and time. The redox reaction between $CuCl_2^-$ and O_2 is assumed to be reversible (Equation (26)). The reverse step accounts for the reduction of Cu^{2+} by O_2-reduction intermediates, such as O_2^- or HO_2^- (Sharma and Millero 1988).

The other homogeneous redox reaction considered in the model is the irreversible reduction of Cu^{2+} by Fe(II). The reaction is assumed to be first order with respect to both $[Cu^{2+}]$ and [Fe(II)] (k_8, Figure 3). Here, the dissolved [Fe(II)] is assumed to be constant. This is equivalent to assuming rapid dissolution of a homogeneously distributed Fe(II)-containing solid. (In a subsequent version of the model (Kolář and King 1996), Equation (24) has been used to predict the release of Fe(II) for a surface-controlled dissolution reaction. This method, however, requires a mass-balance equation for Fe(II) since [Fe(II)] is a function of t, and possibly x).

3.2 EFFECTS OF POROUS MEDIA ON THE CORROSION OF COPPER

The data used for the following analyses are given in Table 1. In each analysis, one or more of the parameters is varied to indicate the effects of the porous medium, adsorption, precipitation or redox reactions on the corrosion behaviour. The variable parameters are identified by shading in the table, along with their median values.

3.2.1 Effect of the Porous Structure

The effect of diffusion through the porous structure on the corrosion rate can be determined by varying one of a number of parameters; ε_e, τ or the length of the diffusion layer L. In addition, the moisture content of the buffer, and hence the degree of saturation (assumed constant in Table 1), can also be varied to determine the effects of rapid O_2 diffusion to the corroding interface.

Figure 5 shows the effect of varying $\varepsilon_e\tau$ on the corrosion rate of Cu in O_2-containing Cl^- environments corresponding to bulk solution ($\varepsilon_e\tau = 1$), a loosely compacted medium ($\varepsilon_e\tau = 0.1$) and compacted buffer material ($\varepsilon_e\tau = 0.01$). As would be expected, the corrosion rate increases with increasing permeability because of the higher rate of mass transport to and from the corroding surface. Figure 6 shows that there is a linear relationship between the corrosion rate and $(\varepsilon_e\tau)^{1/2}$, as would be expected for a mass-transport-limited reaction. A plot of log rate against log time (Figure 7) confirms mass-transport control, as indicated by the slope of 0.5 observed at short times. At longer times, the curve deviates from the slope of 0.5. The point of deviation corresponds to the time at which virtually all the O_2 in the system is consumed. In these simulations, $\varepsilon_e\tau$ was varied by varying τ for a constant value of ε_e. Consequently, the total amount of O_2 in the system, which is determined by the porosity in a porous medium, was the same in each case. Therefore, since the O_2 is consumed faster at $\varepsilon_e\tau = 1.0$, the point at which the log rate vs. log time curve deviates from the slope of -0.5 occurs at a shorter time.

Although these predictions suggest that the corrosion rate is mass-transport limited initially, they do not indicate whether the anodic or the cathodic reaction is rate determining. In bulk solution, experimental

evidence from RDE studies (King et al. 1995a) suggests that the O_2 reduction reaction is kinetically controlled at E_{CORR} in aerated Cl^- solutions, and that it is the anodic reaction that is mass-transport limited (by the diffusion of $CuCl_2^-$ away from the electrode surface). Therefore, it might be supposed that, at least for the simulation for $\varepsilon_e\tau = 1$, the anodic reaction may be the overall rds at short times. However, in these simulations the amount of available O_2 is limited (unlike the case of an RDE immersed in bulk aerated solution) and it must diffuse over a distance of up to 1 m (as opposed to the few tens of μm for an RDE). Therefore, it is more likely in this case that the cathodic reaction is mass-transport limited and is the overall rds. Figure 8 shows the time dependence of the $[O_2]$ profiles for the simulation of a layer of compacted buffer material ($\varepsilon_e\tau = 0.01$). After only 16 d (not shown in Figure 8), the interfacial $[O_2]$ has fallen to 17% of its initial value, indicating significant transport control of the cathodic reaction. The period required to establish complete transport control of the cathodic reaction (defined here as the time required to reduce the interfacial $[O_2]$ to 1×10^{-6} mol·dm^{-3}, 0.5% of the initial value) varies from 0.3 a for $\varepsilon_e\tau = 1$ to ~10 a for $\varepsilon_e\tau = 0.01$. Thus, in systems in which the total amount of O_2 is constant, the period to establish transport control of the cathodic reaction decreases with increasing permeability. If, instead of varying τ we had varied ε_e to give the various rates of mass transport, the time to establish transport control of the cathodic reaction would have increased with increasing permeability because of the greater amount of O_2 trapped in the pores of the porous medium. Figure 8 also shows that some O_2 diffuses out of the buffer into the rock layer. Although the concentration of O_2 in the rock layer is significant, the amount of O_2 that diffuses out of the vault is small because of the lower porosity of the rock (~100 times lower than the porosity of the buffer). Therefore, the rock acts as a significant barrier for both the egress and ingress of O_2.

It appears, therefore, that the most likely rds for the corrosion of Cu in compacted buffer material is the supply of O_2 to the corroding surface. It is possible that, at very short times (shorter than those shown in Figure 7), the anodic mass-transport step may be rate controlling, as found for RDE in bulk solution. The period of anodic mass-transport control would be very short, however, because the O_2 close to the surface would be quickly depleted resulting in a decrease in the interfacial $[O_2]$. Therefore, we must conclude that most of the $t^{-1/2}$ dependence in Figure 7 is due to O_2-transport control. It is also likely that the corrosion rate is cathodically transport limited beyond the time at which the log rate vs. log time curve deviates from the slope of -0.5. As the $[O_2]$ within the porous medium decreases, the amount of O_2 consumed by the homogeneous oxidation of $CuCl_2^-$ becomes more significant. Therefore, at long times, the rate of corrosion is still O_2-transport controlled, but the rate of supply of O_2 to the surface is modified by the homogeneous redox reaction, resulting in a departure from the expected $t^{-1/2}$ dependence.

The rate of mass transport of O_2 to the surface is also affected by the degree of saturation of the porous medium. In unsaturated systems, O_2 diffusion can occur in both the solution- and gas-phases (Equation (10)). Since D_g is about four orders of magnitude higher than D_0, this effect can be significant. Figure 9 compares the depth of corrosion (as the integrated i_{CORR}) as a function of time for fully (S = 1.0) and 80% (S = 0.8) saturated buffer material (King and Kolář 1995). The corrosion rate (which is proportional to the slope of the linearized version of Figure 9) is higher in the partially saturated medium, resulting in faster consumption of the trapped O_2, the amount of which was constant in both simulations. In both cases, corrosion stops once all the trapped O_2 is consumed. In the fully saturated case, slightly less O_2 is reduced on the container surface (lower limiting $\int i_{CORR}$ in Figure 9) because some of the Cu(I) is oxidized for a second time following the slow reduction of Cu(II) by Fe(II) assumed in this calculation (King and Kolář 1995). The effect of decreasing the moisture content by this amount is to increase the effective diffusion coefficient of O_2 (D_{eff}, Equation (10)) from 1.7×10^{-7} cm^2·s^{-1} at S = 1.0 to 1.2×10^{-4} cm^2·s^{-1} at S = 0.8 (King and Kolář 1995). The effect on the diffusion coefficients of $CuCl_2^-$ and Cu^{2+} is minor, resulting in a decrease in $\varepsilon_e\tau D$ from 6×10^{-8} cm^2·s^{-1} at S = 1.0 to 5×10^{-8} cm^2·s^{-1} at S = 0.8. This is further evidence that the overall corrosion rate is cathodically mass-transport controlled, since i_{CORR} increases with decreasing S.

3.2.2 Effect of Adsorption and Precipitation

Reaction (19) indicates that adsorption and precipitation can increase the rate of reversible anodic reactions by decreasing the activity of dissolved M^{n+}. However, because the rate of corrosion is largely O_2-transport controlled in the porous media simulated here, adsorption and desorption have no significant effect on the corrosion rate. Figure 10 shows the predicted corrosion rate of Cu in compacted buffer material as a function of time with and without adsorption and desorption of Cu(II). In fact, the predicted corrosion rate with adsorption is slightly lower than that without adsorption. The reason for this apparent beneficial effect of adsorption is not understood at present.

The predicted profiles for the adsorbed Cu(II) concentration (s_2) provide some evidence about the nature of the adsorption process. First, using the median values of k_{11} and k_{-11}, the maximum predicted value of s_2 is <0.1% of the maximum surface coverage s_2^{max} of 0.085 mol·kg^{-1}. Thus, adsorption could be simulated by a linear process (either kinetic (Equation (13)) or equilibrium (Equation (11))), rather than the Langmuir isotherm used in these simulations. Second, comparison of the predicted value of s_2 with the value calculated from the equilibrium Langmuir isotherm indicates that the adsorption process is not at equilibrium. For instance, for the median-value simulation, the model predicts an interfacial dissolved [Cu(II)] (c_2) of 1.6×10^{-6} mol·dm^{-3} and a corresponding value of s_2^{kin} of 5.2×10^{-5} mol·kg^{-1}, where the superscript kin indicates a value calculated using the kinetic model. In comparison, Equation (12) predicts the equilibrium adsorbed Cu(II) concentration for a Langmuir isotherm to be $s_2^{eq} = 2.7 \times 10^{-4}$ mol·kg^{-1}, ~5 times larger than s_2^{kin} (in Equation (12), $K' = k_{11}/k_{-11}$). Even if k_{11} and k_{-11} are increased by two orders of magnitude, the adsorption process is still predicted not to be at equilibrium. Therefore, the detailed model calculations support the conclusion arrived at from Equations (16) and (18), that the adsorption of Cu(II) by Na-bentonite in compacted buffer material is not an equilibrium process.

3.2.3 Effect of Redox Reactions

The redox reactions considered here are those between Fe(II) and either O_2 or Cu(II) (Equations (26) and (27)). The presence of Fe(II) in compacted buffer material (simulated here by assuming a constant [Fe(II)] of 10^{-5} mol·dm^{-3}) affects both the consumption of O_2 and, through $[CuCl_2^-]$, the variation of E_{CORR} with time. The corrosion potential is calculated from the anodic interfacial expression (Equation (36))

$$E_{CORR} = E_a^0 + \frac{2.3RT}{F} \log\left[\left(\frac{k_{-1}}{n_a F k_1 k_2 [Cl^-]^2}\right)\left(i_{CORR} + n_a F k_{-2}[CuCl_2^-]_0\right)\right] \qquad (40)$$

where i_{CORR} and $[CuCl_2^-]_0$ are calculated by the model.

Figure 11 illustrates the effect of Fe(II) on the depth of corrosion in compacted buffer material for simulations in which there is either no Fe(II) or a constant [Fe(II)] of 10^{-5} mol·dm^{-3}. Because the total amount of O_2 is limited, corrosion stops once all the O_2 is consumed. The effect of Fe(II) is to consume much of the available O_2 by the homogeneous oxidation reaction to produce Fe(III) (Equation (27)). Because this reaction is fast (k_a in Table 1) and because we assume a constant [Fe(II)], most of the O_2 is consumed by this reaction rather than by the corrosion of the container. Although, in practice, the [Fe(II)] will be lower because of the slow dissolution rate of Fe(II) minerals (Kolář and King 1996), this simulation does serve to demonstrate that the presence of Fe(II) will diminish the extent of corrosion of Cu containers.

The faster consumption of O_2 and the reduction of Cu(II) to $CuCl_2^-$ by Fe(II) also affects the time dependence of E_{CORR}. Figure 12 shows the variation of E_{CORR} with time for the two cases considered in the previous figure. In general, E_{CORR} is more negative in the presence of Fe(II), as would be expected. However, the variation of E_{CORR} with time is more complicated because, as Equation (40) indicates, E_{CORR} responds to changes in both i_{CORR} and $[CuCl_2^-]_0$. In the absence of Fe(II) (curve (a), Figure 12), E_{CORR}

decreases with time as i_{CORR} decreases, because of the consumption of O_2. In the presence of Fe(II), the O_2 is almost entirely consumed within 0.1 a. Initially, E_{CORR} decreases due to the decrease in i_{CORR}, but then increases as the Fe(II) reduces Cu(II) to $CuCl_2^-$. Eventually, the interfacial $[CuCl_2^-]$ decreases as $CuCl_2^-$ diffuses away from the interface, resulting in a gradual decrease of E_{CORR} with time.

4. APPLICATION TO OTHER CORROSION SYSTEMS

The modelling techniques developed for the corrosion of Cu in porous buffer material may be applicable to a number of other corrosion systems, such as the effects of corrosion product films on localized corrosion, the adsorption of solutes by corrosion products, and the adsorption of solutes and certain other effects of biofilms.

4.1 EFFECTS OF CORROSION PRODUCT FILMS

4.1.1 Localized Corrosion

Sato (1987) has identified three classes of hydrated metal oxide precipitate membranes: anion-selective, cation-selective and bipolar. Anion-selective films have a positive fixed surface charge, cation-selective films have a negative surface charge and bipolar membranes have a layered structure of both positively and negatively charged surfaces. From membrane-potential measurements, it was found that anions migrated preferentially through anion-selective membranes and vice versa. The selectivity of the membranes could be changed by changing the pH (increasing pH resulted in a change from anion selectivity to cation selectivity) or by the adsorption of charged species (the adsorption of MoO_4^{2-}, for example, changed an anion-selective membrane into a cation-selective layer, Sakashita and Sato 1979).

Sato (1987) considered the migration of charged species across the membranes due to the difference in potential across the layer. Migration of charged species is also believed to occur in localized corrosion because of the difference in potential caused by the separation of anodic and cathodic sites. Migration is not considered in Equation (1) since it was developed for a uniform corrosion reaction and because membrane potentials across clay layers have been shown to be small (<20 mV, King et al. 1995a). However, migration could be accounted for by including an additional term describing the potential drop across the diffusion layer. Since anions were found to be preferentially transported through membranes with positive surface charge, surface diffusion (which is included in Equation (1)) may also have occurred within these membranes.

Suleiman et al. (1994) report experimental evidence to support the idea that anion-selective membranes can enhance localized corrosion. Stable pitting of stainless steel was observed in the presence of a rust membrane at potentials and/or $[Cl^-]$ lower than those necessary to induce pitting on membrane-free surfaces. The results were interpreted in terms of the preferential migration of Cl^- ions across the anion-selective rust membrane, as suggested by Sato. An additional effect was claimed to be the lower resistance to current flow through the pores of the membrane.

It is also possible that porous layers with positive surface charge (equivalent to the anion-selective membranes discussed above) could prevent or inhibit corrosion. In the absence of migration or surface diffusion, Equation (1) predicts that the transport of Cl^- through a positively charged layer would be retarded by the effects of adsorption and/or precipitation. Alternatively, negatively charged surfaces could delay the initiation of localized corrosion by adsorbing dissolved cations and preventing acidification of the occluded region by hydrolysis of M^{n+}. In both cases, however, adsorption will only alter the pore-water composition as long as the surfaces sites are not saturated by adsorbates. In the concentrated solutions that develop within occluded regions, it is quite possible that either positively or negatively charged surface layers could be saturated by adsorbate.

An associated effect is the hideout of solute species in oxide-filled cracks and crevices in steam generators (Balakrishnan, private communication). Anionic species such as SO_4^{2-} and PO_4^{2-} are known to accumulate in oxide layers during operation. This concentration effect may be a problem in itself, causing localized corrosion of the underlying structure. When attempts are made to leach these solutes from the plant (so-called hideout return), they do not do so congruently. In other words, one solute leaches from the porous layer preferentially. Assuming the species were both uniformly distributed initially and that their diffusion coefficients are approximately equal, this difference in leach rates can only be explained by preferential adsorption of one of the solutes. This effect could be simulated using Equation (1) by taking into account the competitive adsorption of the two adsorbates. The most straightforward method of modelling competitive adsorption is by using kinetic adsorption models. The species that is less strongly retarded by adsorption would have a lower rate of adsorption and a higher rate of desorption than the more strongly sorbed species.

4.1.2 Modelling of Biofilms

Certain aspects of the interaction between biofilms and metal surfaces could also be modelled using Equation (1). In most cases, however, biofilm formation is patchy, with some areas of the surface covered by a relatively thick, adherent biofilm and others covered by a thinner biofilm or by no film at all (Angell et al. 1995). The most damaging forms of microbially influenced corrosion (MIC) are usually associated with non-uniform biofilms, with heavily covered parts of the surface becoming anodic to the "bare" parts of the surface. Here, we shall only consider effects of uniform biofilms.

Biofilms can be viewed as layered structures with a gradation in the environment through the film. Thus, the inner surface of the biofilm might be anoxic, supporting the growth of anaerobic microbes, whilst the outer layer exposed to the aerated bulk environment could be oxic and be populated by aerobic species (Little et al. 1991). The gradation in $[O_2]$ in a model biofilm has been verified experimentally (Lewandowski et al. 1989). This type of structure could be modelled using Equation (1) and a number of different layers. Redox reactions characteristic of anaerobic bacteria could be included in the inner layer and reactions characteristic of aerobic bacteria in the outer layer, closest to the source of O_2. By varying the microbial population in the various layers, the effectiveness of the microbial reactions in maintaining the gradation of $[O_2]$ through the biofilm could be predicted.

In some cases of MIC, the formation of a biofilm is thought to reduce the rate of corrosion by slowing the supply of O_2 to the metal surface (Schiffrin and de Sanchez 1985). Such effects could easily be modelled using a diffusion equation, with or without reaction terms, provided the thickness and porosity of the biofilm are known. Attempts have been made to measure these parameters for both ideal and natural biofilms using O_2-reduction measurements of biofilm-covered Au rotating disc and hydrodynamically modulated RDE (L'Hostis et al. 1995). For the natural biofilm, the film thickness was found to be ~5 μm.

Biofilms have also been found to adsorb dissolved metal ions (Geesey et al. 1986). The adsorptive part of the biofilm is the extracellular polymeric substance (EPS) excreted by the microbes, rather than the microbes themselves. It has been found that when exposed to toxic ions such as Cu^{2+}, microbes increase their EPS production in order to lower the dissolved ion concentration (Wagner et al. 1991). As with the adsorption of Cu(II) by Na-bentonite, adsorption of Cu(II) by EPS has been shown to increase the rate of corrosion (Geesey et al. 1986). Again, these effects are easily modelled, provided the kinetic adsorption/desorption rate constants or equilibrium adsorption isotherms are known.

5. CONCLUSIONS

The geochemical literature is full of references to mass transport through porous media and the effects of adsorption, precipitation and redox processes. Much of this information can be applied to the corrosion of materials in porous media. Examples of these various processes have been discussed, with the

emphasis on the presentation of equations that can be included in predictive corrosion models. The effects of diffusion in porous materials and adsorption, precipitation and redox processes have been illustrated using a kinetically based model for the prediction of the long-term corrosion behaviour of Cu nuclear waste containers in a conceptual Canadian disposal vault. The corrosion rate of Cu containers has been shown to be largely controlled by the rate of supply of O_2 to the corroding surface. Consequently, the corrosion rate increases with increasing permeability of the porous medium. Adsorption and precipitation, which can increase the rate of reversible anodic dissolution reactions, have no effect on the corrosion rate because it is under cathodic transport control. The addition of Fe(II), which can consume O_2 and reduce Cu(II) to Cu(I) in homogeneous redox reactions, leads to lower corrosion rates and E_{CORR} because of the consumption of O_2 and the creation of more reducing conditions within the disposal vault.

ACKNOWLEDGEMENT

The Canadian Nuclear Fuel Waste Management Program is jointly funded by AECL and Ontario Hydro through the CANDU Owners Group.

REFERENCES

AECL. 1994. Environmental impact statement on the concept for disposal of Canada's nuclear fuel waste. Atomic Energy of Canada Limited Report, AECL-10711, COG-93-1.

Angell, P., A. Sonnerson, P. Wagner, D.C. White and B. Little. 1995. The role of *Oceanospirillum* exopolymer in marine copper corrosion. In Proc. 1995 Int. Conf. on Microbially Influenced Corrosion, NACE International and American Welding Society, Houston, TX and Miami, FL, p. 74/1-74/7.

Cho, W.J., D.W. Oscarson, M.N. Gray and S.C.H. Cheung. 1993. Influence of diffusant concentration on diffusion coefficients in clay. Radiochim. Acta 60, 159-163.

Collin, M. and A. Rasmuson. 1988. A comparison of gas diffusivity models for unsaturated porous media. Soil Sci. Soc. Am. J. 52, 1559-1565.

Conca, J.L. and J. Wright. 1991. Aqueous diffusion coefficients in unsaturated materials. In Scientific Basis for Nuclear Waste Management XIV, T. Abrajano Jr. and L.H. Johnson eds. (Mater. Res. Soc. Symp. Proc. 212, Pittsburgh, PA), 879-884.

Cook, A.J. 1988. A desk study of surface diffusion and mass transport in clay. British Geological Survey Report, WE/88/34.

Craig, R.F. 1987. Soil Mechanics, 4th ed., Van Nostrand Reinhold, London.

Garisto, N.C. and F. Garisto. 1986. The effect of precipitation on the long-term release of radionuclides from used fuel. Ann. Nucl. Energy 13, 591-596.

Geesey, G.G., M.W. Mittelman, T. Iwaoka and P.R. Griffith. 1986. Role of bacterial exopolymers in the deterioration of metallic copper surfaces. Mater. Perform. 25, 37-40.

Haworth, A. 1990. A review of the modelling of sorption from aqueous solution. Adv. Colloid Interface Sci. 32, 43-78.

Johnson, L.H., J.C. Tait, D.W. Shoesmith, J.L. Crosthwaite and M.N. Gray. 1994a. The disposal of Canada's nuclear fuel waste: engineered barriers alternatives. Atomic Energy of Canada Limited Report, AECL-10718, COG-93-8.

Johnson, L.H., D.M. LeNeveu, D.W. Shoesmith, D.W. Oscarson, M.N. Gray, R.J. Lemire and N.C. Garisto. 1994b. The disposal of Canada's nuclear fuel waste: the vault model for postclosure assessment. Atomic Energy of Canada Limited Report, AECL-10714, COG-93-4.

Kato, C., B.G. Ateya, J.E. Castle and H.W. Pickering. 1980a. On the mechanism of corrosion of Cu-9.4Ni-1.7Fe alloy in air saturated aqueous NaCl solution. I. Kinetic investigations. J. Electrochem. Soc. 127, 1890-1896.

Kato, C., J.E. Castle, B.G. Ateya and H.W. Pickering. 1980b. On the mechanism of corrosion of Cu-9.4Ni-1.7Fe alloy in air saturated aqueous NaCl solution. II. Composition of the protective surface layer. J. Electrochem. Soc. 127, 1897-1903.

King, F. 1987. A technique to investigate the mechanism of uniform corrosion in the presence of a semi-permeable membrane. Atomic Energy of Canada Limited Report, AECL-9064.

King, F. 1996. A model for the corrosion of copper containers in a Canadian nuclear fuel waste disposal vault. Part 1. The corrosion model. Atomic Energy of Canada Limited Report, AECL-11472, COG-95-520.

King, F. and M. Kolář. 1995. Prediction of the lifetimes of copper nuclear waste containers under restrictive mass-transport and evolving redox conditions. CORROSION/95, paper no. 425, NACE International, Houston, TX.

King, F., C.D. Litke and S.R. Ryan. 1992. A mechanistic study of the uniform corrosion of copper in compacted Na-montmorillonite/sand mixtures. Corros. Sci. 33, 1979-1995.

King, F., C.D. Litke, M.J. Quinn and D.M. LeNeveu. 1995a. Measurement and prediction of the corrosion potential of copper in chloride solutions as a function of oxygen concentration and mass-transfer coefficient. Corros. Sci. 37, 833-851.

King, F., C.D. Litke and Y. Tang. 1995b. Effect of interfacial pH on the reduction of oxygen on copper in neutral $NaClO_4$ solution. J. Electroanal. Chem. 384, 105-113.

King, F., M.J. Quinn and C.D. Litke. 1995c. Oxygen reduction on copper in neutral NaCl solution. J. Electroanal. Chem. 385, 45-55.

Kolář, M. and F. King. 1996. Modelling the consumption of oxygen by container corrosion and reaction with Fe(II). In Scientific Basis for Nuclear Waste Management XIX, W.M. Murphy and D. Knecht eds. (Mater. Res. Soc. Symp. Proc. 412, Pittsburgh, PA), 547-554.

Koopman, D.C., J.V. Cole and H.H. Lee. 1992. Assumption of local equilibrium in adsorption processes. AIChE J. 38, 623-625.

Lewandowski, Z., W.C. Lee, W.G. Characklis and B. Little. 1989. Dissolved oxygen and pH microelectrode measurements at water-immersed metal surfaces. Corrosion 45, 92-98.

L'Hostis, E., C. Compère, D. Festy, B. Tribollet and C. Deslouis. 1995. Characterization of biofilms formed on gold in natural seawater by the oxygen diffusion analysis. Proc. 1995 Int. Conf. on Microbially Influenced Corrosion, NACE International and American Welding Society, Houston, TX and Miami, FL, p. 60/1-60/11.

Little, B., P. Wagner and F. Mansfeld. 1991. Microbiologically influenced corrosion of metals and alloys. Int. Mater. Rev. 36, 253-272.

Macdonald, D.D. and M. Urquidi-Macdonald. 1990. Thin-layer mixed-potential model for the corrosion of high-level nuclear waste containers. Corrosion 46, 1990, 380-390.

Malmström, M., S. Banwart, L. Duro, P. Wersin and J. Bruno. 1995. Biotite and chlorite weathering at 25°C. Swedish Nuclear Fuel and Waste Management Company Technical Report, TR 95-01.

Mancey, D.S., D.W. Shoesmith, J. Lipkowski, A.C. McBride and J. Noël. 1993. An electrochemical investigation of the dissolution of magnetite in acidic electrolytes. J. Electrochem. Soc. 140, 637-642.

Oscarson, D.W. 1994. Surface diffusion: is it an important transport mechanism in compacted clays? Clays Clay Miner. 42, 534-543.

Oscarson, D.W. and D.A. Dixon. 1989. Elemental, mineralogical, and pore-solution composition of selected Canadian clays. Atomic Energy of Canada Limited Report, AECL-9891.

Oscarson, D.W., H.B. Hume, N.G. Sawatsky and S.C.H. Cheung. 1992. Diffusion of iodide in compacted bentonite. Soil Sci. Soc. Am. J. 56, 1400-1406.

Oscarson, D.W., H.B. Hume and F. King. 1994. Sorption of cesium on compacted bentonite. Clays Clay Miner. 42, 731-736.

Peters, D.G. and S.A. Cruser. 1965. Cathodic chronopotentiometry of copper(I) and copper(II) in chloride media. J. Electroanal. Chem. 9, 27-40.

Ryan, S.R. and F. King. 1994. The adsorption of Cu(II) on sodium bentonite in a synthetic saline groundwater. Atomic Energy of Canada Limited Report, AECL-11062, COG-94-125.

Sato, N. 1987. Some concepts of corrosion fundamentals. Corros. Sci. 27, 421-433.

Sakashita, M. and N. Sato. 1979. Ion selectivity of precipitate films affecting passivation and corrosion of metals. Corrosion 35, 351-355.

Schiffrin, D.J. and S.R. de Sanchez. 1985. The effect of pollutants and bacterial microbiofouling on the corrosion of copper base alloys in seawater. Corrosion 41, 31-38.

Sharma, V.K. and F.J. Millero. 1988. The oxidation of Cu(I) in electrolyte solutions. J. Solution Chem. 17, 581-599.

Shoesmith, D.W. and S. Sunder. 1992. The prediction of nuclear fuel (UO_2) dissolution rates under waste disposal conditions. J. Nucl. Mater. 190, 20-35.

Stumm, W. 1992. Chemistry of the Solid-water Interface, Wiley-Interscience, New York.

Suleiman, M.I., I. Ragault and R.C. Newman. 1994. The pitting of stainless steel under a rust membrane at very low potentials. Corros. Sci. 36, 479-486.

Travis, C.C. 1978. Mathematical description of adsorption and transport of reactive solutes in soils: a review of selected literature. Oak Ridge National Laboratory Report, ORNL-5403.

Vazquez, M.V., S.R. de Sanchez, E.J. Calvo and D.J. Schiffrin. 1994. The electrochemical reduction of oxygen on polycrystalline copper in borax buffer. J. Electroanal. Chem. 374, 189-197.

Wagner, P.A., B.J. Little and A.V. Stiffey. 1991. An electrochemical evaluation of copper colonized by a copper-tolerant marine bacterium. CORROSION/91, NACE International, Houston, TX, paper 109.

Werme, L., P. Sellin and N. Kjellbert. 1992. Copper canisters for nuclear high level waste disposal. Corrosion aspects. Swedish Nuclear Fuel and Waste Management Company Technical Report, TR 92-26.

Wersin, P., K. Spahiu and J. Bruno. 1994. Time evolution of dissolved oxygen and redox conditions in a HLW repository. Swedish Nuclear Fuel and Waste Management Company Technical Report, TR 94-02.

Williamson, M.A. and J.D. Rimstidt. 1994. The kinetics and electrochemical rate-determining step of aqueous pyrite oxidation. Geochim. Cosmochim. Acta 58, 5443-5454.

TABLE 1

MEDIAN VALUES OF PARAMETERS IN COPPER CORROSION MODEL*

Parameter	Definition	Median Value
c_1^{sat}	Equilibrium c_1^s in contact with Cu(I) solid	1×10^{-4} mol·dm^{-3}
c_2^{sat}	Equilibrium c_2^s in contact with Cu(II) solid	1.7×10^{-7} mol·dm^{-3}
c_3^s	**Dissolved Fe(II) concentration in pore water**	**1×10^{-5} mol·dm^{-3}**
c_{buffer}	Initial pore-water O_2 concentration in buffer	2×10^{-4} mol·dm^{-3}
c_{rock}	O_2 concentration in rock	3.1×10^{-7} mol·dm^{-3}
k_a	Rate of O_2 reaction with Fe(II)	2.9 dm^3·mol^{-1}·s^{-1}
k_5	Rate of dissolution of Cu_2O	0.1 s^{-1}
k_{-5}	Rate of hydrolysis of $CuCl_2^-$	1 s^{-1}
k_7	Rate of oxidation of Cu(I)	29 dm^3·mol^{-1}·s^{-1}
k_{-7}	Rate of reduction of Cu(II) by peroxide	10^{-4} s^{-1}
k_8	Rate of reduction of Cu(II) by Fe(II)	1 dm^3·mol^{-1}·s^{-1}
k_9	**Rate of precipitation of Cu(II)**	**1×10^{-6} s^{-1}**
k_{-9}	**Rate of dissolution of Cu(II) solid**	**1×10^{-6} s^{-1}**
k_{11}	**Rate of adsorption of Cu(II)**	**2×10^{-3} dm^3·mol^{-1}·s^{-1}**
k_{-11}	**Rate of desorption of Cu(II)**	**1×10^{-6} s^{-1}**
n_c	Number of electrons for O_2 reduction	4
n_a	Number of electrons for Cu dissolution	1
s_2^{max}	Maximum sorbed Cu(II) concentration	0.085 mol·kg^{-1}
k^{**}	Electrochemical constant	0.2065 A^3·mol^{-2}
k_{-2}	Electrochemical rate constant	1370 A·cm·mol^{-1}
E_a^0	Standard potential for anodic reaction	-0.105 V_{SCE}
$k_{-1}/n_aFk_1k_2[Cl^-]^2$	Electrochemical rate constant term	6.28 cm^2·A^{-1}
D_0^s	Bulk-solution diffusion coefficient of O_2	1.7×10^{-5} cm^2·s^{-1}

TABLE 1 (concluded)

MEDIAN VALUES OF PARAMETERS IN COPPER CORROSION MODEL

Parameter	Definition	Median Value
D_1	Bulk-solution diffusion coefficient of Cu(I)	5.5×10^{-6} cm^2·s^{-1}
D_2	Bulk-solution diffusion coefficient of Cu(II)	6×10^{-6} cm^2·s^{-1}
D_g	Gas-phase diffusion coefficient of O_2	0.178 cm^2·s^{-1}
D_{eff}	Effective diffusion coefficient of O_2 in buffer	1.7×10^{-7} cm^2·s^{-1}
F	Faraday constant	96 487 C·mol^{-1}
L	Length of diffusion layer	1 m
R	Gas constant	8.314 J·K^{-1}·mol^{-1}
T	Absolute temperature	298.2 K
ε_a	Accessible porosity ($\varepsilon_a = \varepsilon_e + \varepsilon_s$)	0.2
ε_e	Effective porosity	0.1
ε_s	Storage porosity	0.1
ρ	Dry density of buffer material	1.65 g·cm^{-3}
κ_{eq}	Ratio of gas- to solution-phase [O_2]	42.7
τ_g	Tortuosity factor of gas-filled pores in buffer material	0.1
τ	**Tortuosity factor of solution-filled pores in buffer material**	**0.1**

* Assumed conditions: 25°C, S = 1.0 (fully saturated), [Cl$^-$] = 1 mol·dm^{-3}.

** $$k = n_a F \left(\frac{k_1 k_2}{k_{-1}} \right) \left(n_c F k_c^0 \right)^2 \left[Cl^- \right]^2 \exp\left[\frac{F}{RT} \left(E_c^0 - E_a^0 \right) \right]$$

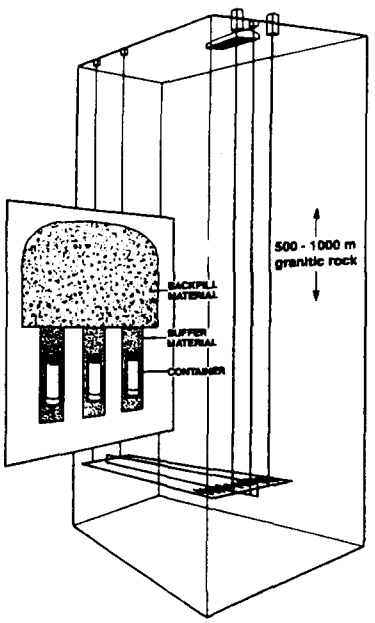

FIGURE 1: Illustration of the Concept for the Disposal of Nuclear Fuel Waste in Canada. The containers are surrounded by a number of engineered and natural barriers, including buffer and backfill materials and 500-1000 m of granitic rock.

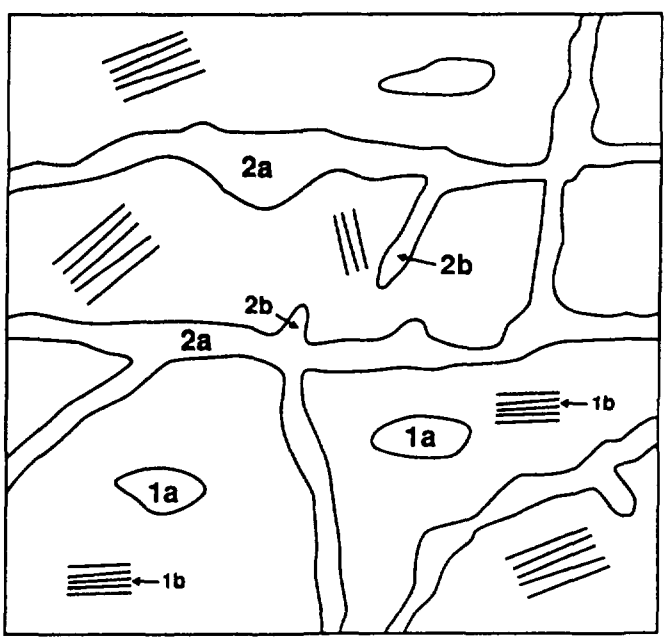

FIGURE 2: Schematic Showing the Different Types of Porosity in Compacted Buffer Material. The non-accessible porosity (ε_{na}) consists of isolated pores (1a) and inter-lamellar spaces between clay particles (1b) that are too small for solutes to enter. The accessible porosity (ε_a) consists of the effective porosity (ε_e, 2a), comprising interconnected through pores that contribute to mass transport through the buffer, and storage porosity (ε_s, 2b), comprising dead-end pores.

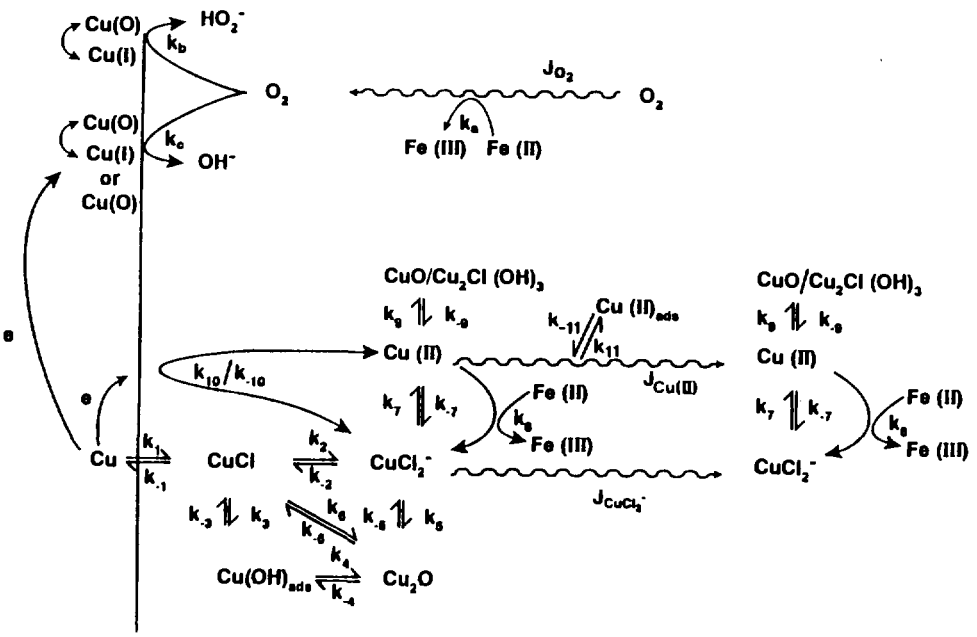

FIGURE 3: Reaction Mechanism Proposed for the Corrosion of Copper Nuclear Fuel Waste Containers in a Canadian Disposal Vault (King and Kolář 1995).

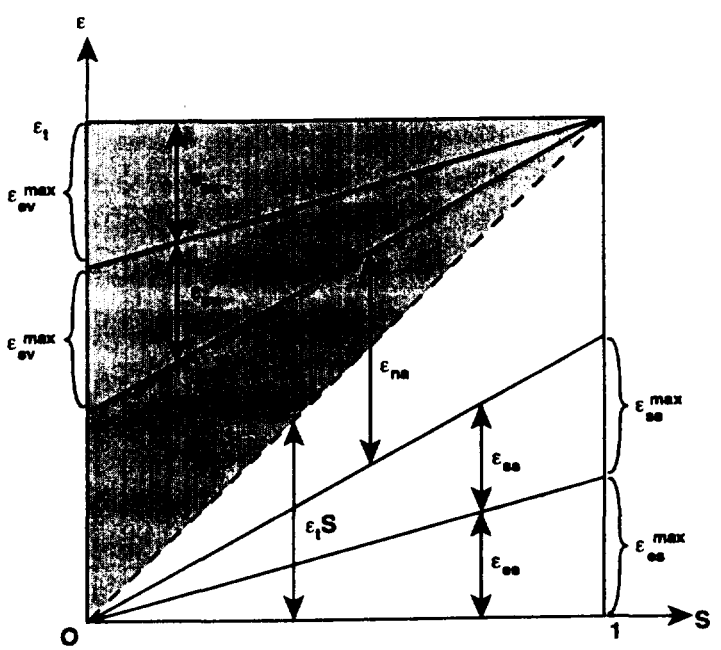

FIGURE 4: Assumed Variation of Various Porosities Associated with Mass Transport Through Buffer Material as a Function of the Degree of Saturation S. ε_{ns}, ε_e and ε_s are defined in Figure 2, ε_t is the total porosity and subscripts v and s refer to gas- (or vapour-) phase and solution-phase porosities, respectively.

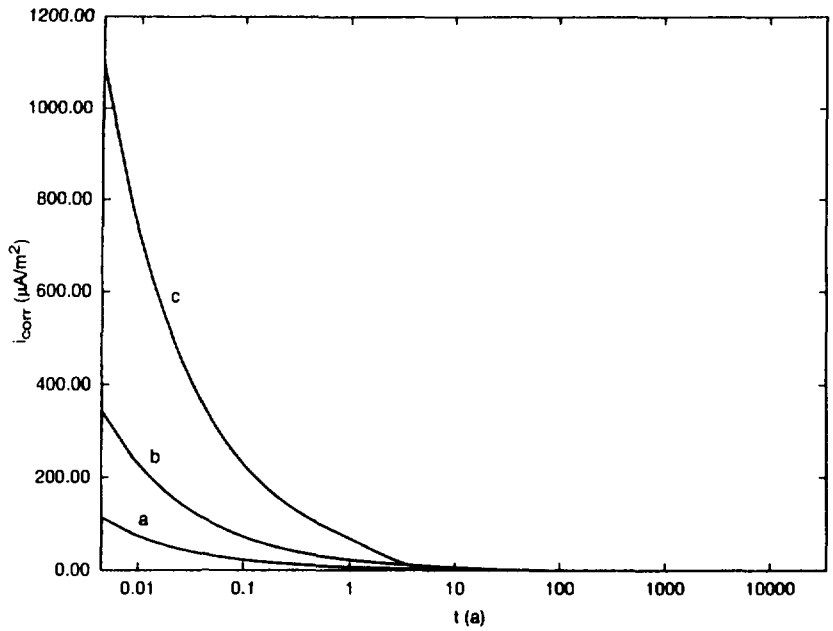

FIGURE 5: The Effect of the Permeability ($\varepsilon_e\tau$) of Compacted Buffer Material on the Corrosion Rate of Copper. The permeability was varied by varying the tortuosity factor τ to give $\varepsilon_e\tau$ values of (a) 0.01, (b) 0.1 and (c) 1.0, representative of compacted buffer material, partially compacted buffer material and bulk solution, respectively. In the simulation, the corroding surface was surrounded by a 1-m diffusion layer saturated with 1 mol·dm^{-3} Cl^- solution containing a constant amount of O_2 at 25°C.

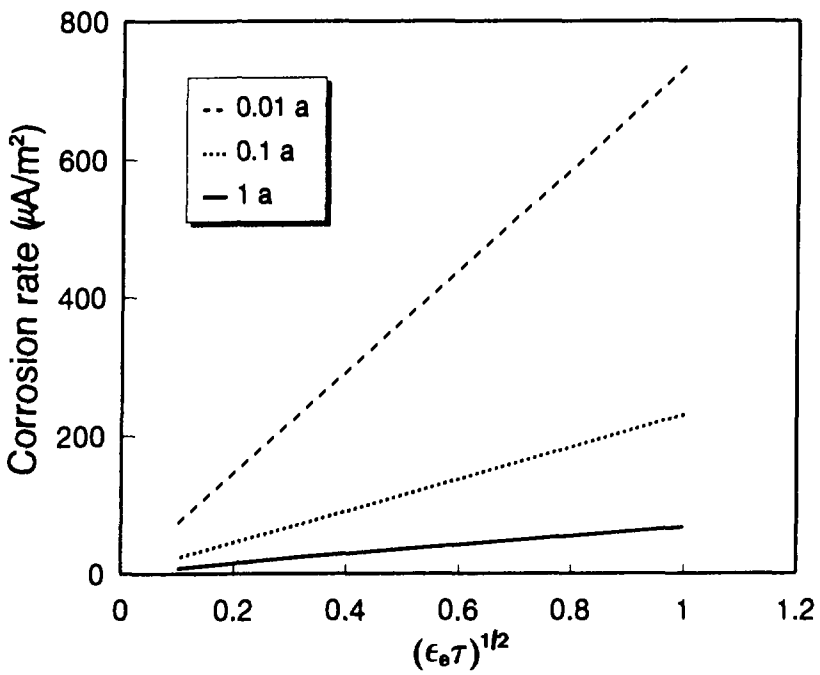

FIGURE 6: The Dependence of the Corrosion Rates from Figure 5 on $(\varepsilon_e\tau)^{1/2}$ at Various Selected Times. The linear dependence suggests transport control of the corrosion reaction.

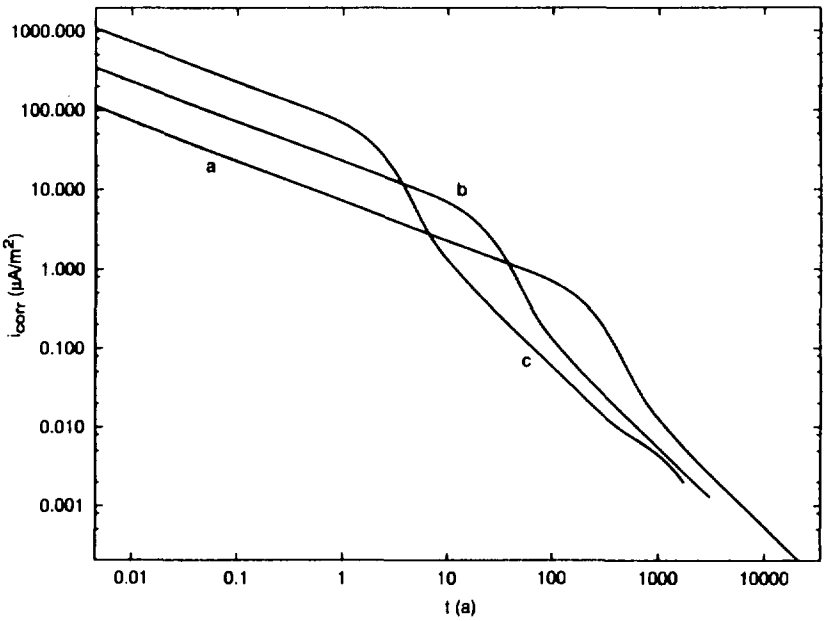

FIGURE 7: The Data from Figure 5 Plotted in the Double Logarithmic Form. The slope of -0.5 at short times suggests the corrosion rate is transport controlled.

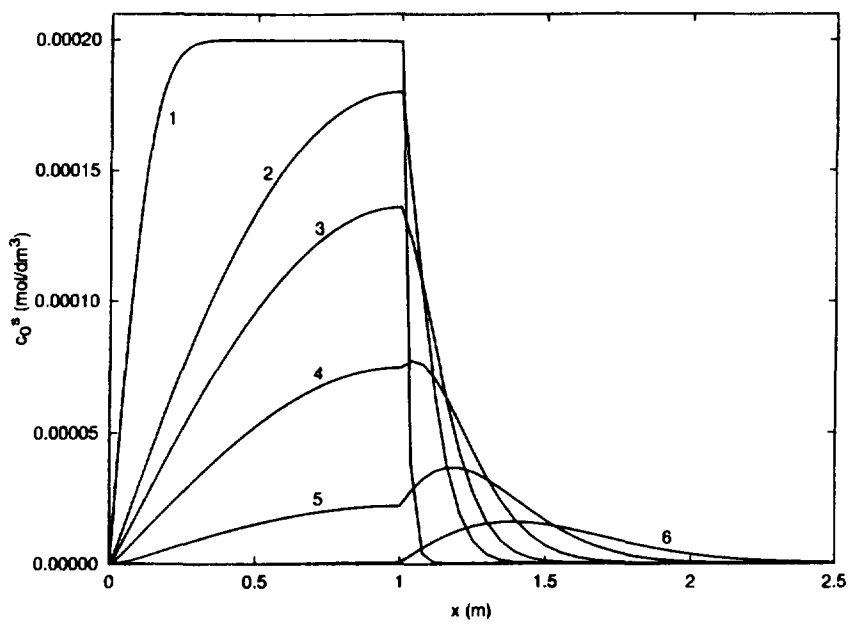

FIGURE 8: The Spatial Distribution of Dissolved Oxygen as a Function of Time for a 1-m Thick Layer of Compacted Buffer Material. (1) 2.2 a, (2) 4.8 a, (3) 9.3 a, (4) 18.3 a, (5) 35.9 a, and (6) 70.4 a. Same conditions as Figure 5 for $\varepsilon_e\tau$ = 0.01.

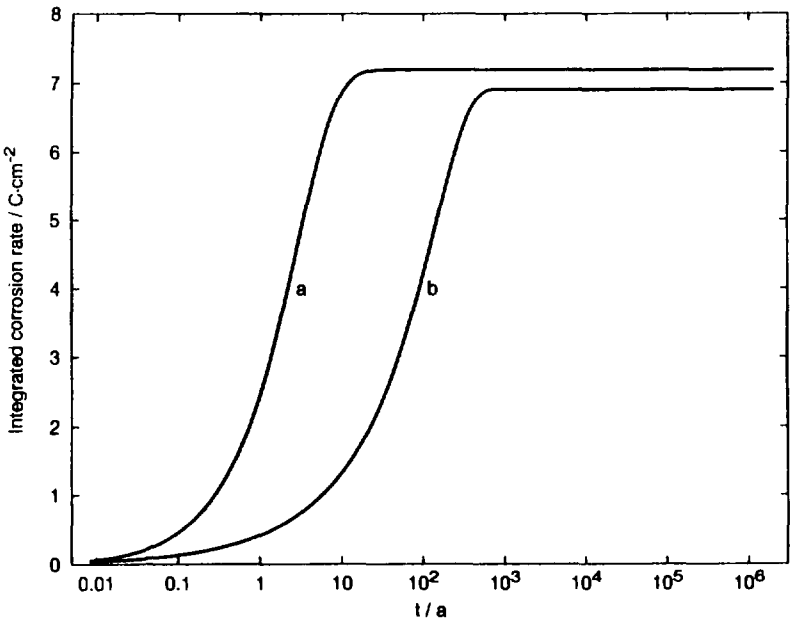

FIGURE 9: The Effect of the Degree of Saturation on the Time Dependence of the Depth of Corrosion at 25°C. (a) 80% saturated, S = 0.8, and (b) fully saturated (S = 1.0) buffer material (King and Kolář 1995).

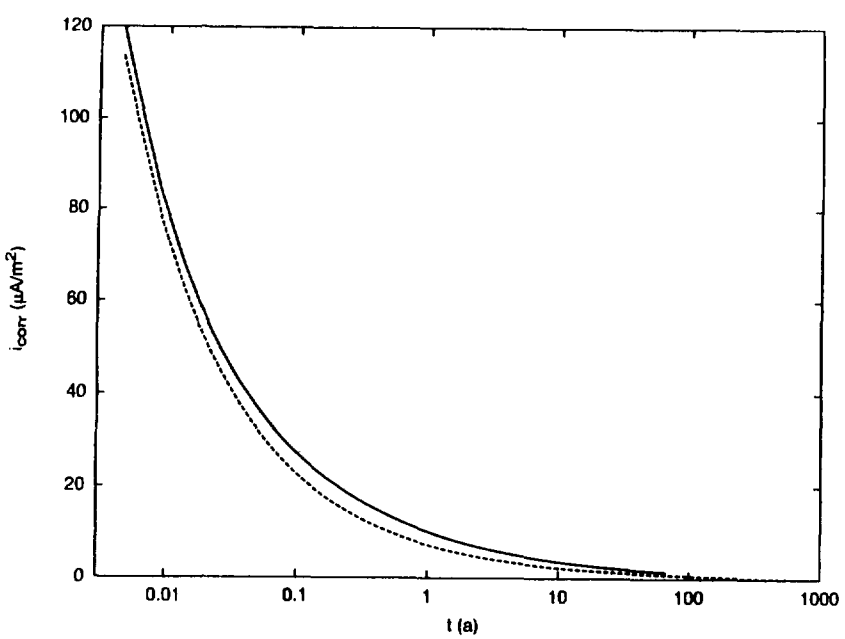

FIGURE 10: Effect of Adsorption on the Corrosion Rate of Copper in Contact with Compacted Buffer Material. Solid line represents no adsorption or desorption and the broken line is for k_{11} = 2 x 10^{-3} dm^3·mol^{-1}·s^{-1} and k_{-11} = 1 x 10^{-6} s^{-1}.

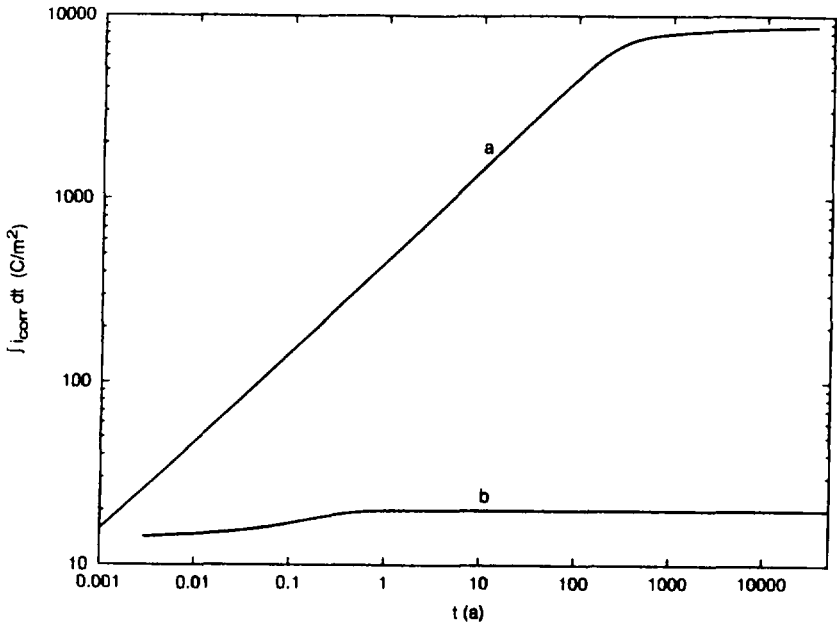

FIGURE 11: Effect of Fe(II) on the Extent of Corrosion of Copper in Compacted Buffer Material. (a) no Fe(II), (b) 10^{-5} mol·dm^{-3} Fe(II).

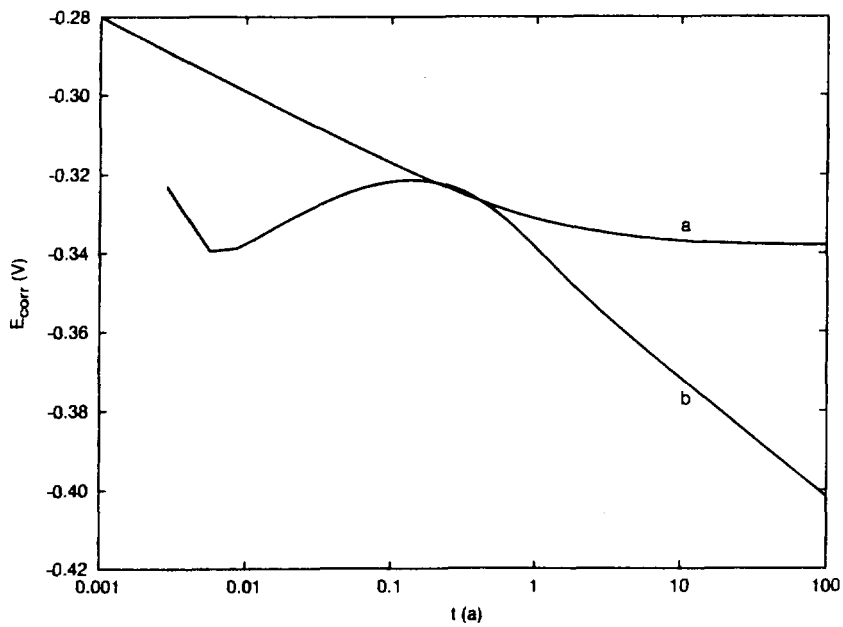

FIGURE 12: Effect of Fe(II) on the Corrosion Potential of Copper in Compacted Buffer Material. (a) no Fe(II), (b) 10^{-5} mol·dm^{-3} Fe(II).

Cat. No. / Nº de cat.: CC2-11592E
ISBN 0-660-16583-X
ISSN 0067-0367

To identify individual documents in the series, we have assigned an AECL- number to each. Please refer to the AECL- number when requesting additional copies of this document from

Scientific Document Distribution Office (SDDO)
AECL
Chalk River, Ontario
Canada K0J 1J0

Fax: (613) 584-1745 Tel.: (613) 584-3311
ext. 4623

Price: A

Pour identifier les rapports individuels faisant partie de cette série, nous avons affecté un numéro AECL- à chacun d'eux. Veuillez indiquer le numéro AECL- lorsque vous demandez d'autres exemplaires de ce rapport au

Service de Distribution des documents officiels (SDDO)
EACL
Chalk River (Ontario)
Canada K0J 1J0

Fax: (613) 584-1745 Tél.: (613) 584-3311
poste 4623

Prix: A